Measurement of the $B_s^0 \to K^+K^-$ lifetime relative to the $B_d^0 \to K^+\pi^-$ lifetime

Public Note

Reference: LHCb-PUB-2009-023
Created: May 12, 2009
Last modified: November 5, 2009

Prepared by: H. Cliff[a], V. Gibson[a], U. Kerzel[a]

[a]Cavendish Laboratory (HEP),
JJ Thomson Avenue,
Cambridge, CB3 0HE

Abstract

The study of B decays to charmless charged hadrons offers an opportunity to improve our understanding CP violation and to search for New Physics beyond the Standard Model. A measurement of the lifetime of the decay $B_s^0 \to K^+K^-$ has the potential to offer insight into both these areas. We have developed an analysis to make a relative measurement of the $B_s^0 \to K^+K^-$ lifetime which removes systematic bias introduced by the use of impact parameter based online and offline selections. This is achieved by fitting the ratio of the proper lifetime distributions of the decay modes $B_s^0 \to K^+K^-$ and $B_d^0 \to K^+\pi^-$ using the best current measurement of the mean B_d^0 lifetime. Combined with other measurements we can then calculate the width in the B_s system $\Delta\Gamma_s$ and compare to the Standard Model prediction and thereby infer the presence of any New Physics. The use of our analysis on simulated events has produced a result of:

$$\tau_{B_s \to KK} = (1.40 \pm 0.05_{stat}) \text{ ps}$$

with

$$\tau_{B_s \to KK\ input} = 1.461 \text{ ps}$$

where the statistical error corresponds to an integrated luminosity of 260 pb^{-1}. Simulation has demonstrated that the method is unbiased and that it may be used early in data taking. The technique is also capable of measuring the mean B_s^0 lifetime through the channel $B_s^0 \to K^-\pi^+$ and the lifetime of the Λ_b^0 baryon through the channels $\Lambda_b^0 \to K^-p^+$ and $\Lambda_b^0 \to \pi^-p^+$.

Contents

1 Introduction 3
1.1 Theoretical overview and present experimental status 3
1.2 LHC*b* Monte Carlo simulation data samples 6
2 Measuring the $B_s \to KK$ lifetime 6
2.1 Overview 6
2.2 Event selection 7
2.3 Mass fit 11
2.3.1 Invariant mass line shapes 12
2.3.2 Fit to the complete invariant mass distribution 14
2.3.3 Implementation 15
2.4 Lifetime extraction 15
3 Toy Monte Carlo simulation studies 17
3.1 Toy model 17
3.2 Results of the standard analysis 19
3.3 Statistics versus precision 22
3.4 Proper lifetime binning 23
3.4.1 Bin shapes 23

3.4.2 Number of bins 23
4 LHC*b* Monte Carlo simulation studies 24
4.1 Results of the standard analysis 24
4.2 Evaluation of systematic uncertainties 26
5 Conclusions 31
6 References 32

1 Introduction

The LHC*b* experiment [1] at the Large Hadron Collider (LHC) [2] at CERN has been constructed to study the phenomenon of CP violation and other rare physical processes through the decay of B mesons. The LHC*b* collaboration will be able to study a larger sample of B_s^0 mesons than has been accumulated at any other experiment.

This note describes an analysis that has been developed to make an unbiased measurement of the $B_s^0 \to K^+K^-$ lifetime at LHC*b*. The motivation for this measurement follows in this section. Section 2 describes the method used by this analysis. We present the results of Toy simulation and LHC*b* simulation studies in Sections 3 and 4, respectively. In Section 5 we draw conclusions and discuss what further work remains to be carried out.

1.1 Theoretical overview and present experimental status

This summary follows the discussion summarised in [3,4].

The evolving $B_s - \bar{B}_s$ system is governed by the Schrödinger equation:

$$i\frac{d}{dt}\begin{pmatrix}|B_s(t)\rangle \\ |\overline{B_s}(t)\rangle\end{pmatrix} = \left(M_s - \frac{i}{2}\Gamma_s\right)\begin{pmatrix}|B_s(t)\rangle \\ |\bar{B}_s(t)\rangle\end{pmatrix} \quad (1)$$

with the mass matrix M_s and the decay matrix Γ_s. The physical eigenstates $|B_H\rangle$ and $|B_L\rangle$ with masses M_H , M_L and decay rates Γ_H, Γ_L are obtained by diagonalising $M_s - i\Gamma_s/2$. For the scope of this analysis, the quantity:

$$\Delta\Gamma_s = \Gamma_L - \Gamma_H = 2|\Gamma_{12}|\cos\Phi_{M/\Gamma} \quad (2)$$

is of particular importance. Within the Standard Model, $\Phi_{M/\Gamma}^{SM} = (4.1 \pm 1.4)\cdot 10^{-3}$, i.e. $\cos\Phi_{M/\Gamma}^{SM} \approx 1$ to good accuracy. It is important to note that new physics cannot affect Γ_{12} which is dominated by CKM-favoured $b \to c\bar{c}s$ tree level decays. Hence all possible effects of new physics affecting $\Delta\Gamma_s$ have to enter via the phase $\Phi_{M/\Gamma}$. This can be expressed as:

$$\Delta\Gamma_s^{meas} = 2\left|\Gamma_{12}^{SM}\right|\cos(\Phi_{M/\Gamma}^{SM} + \Phi^{\Delta}) \quad (3)$$

and new CP violating contributions always *reduce* $\Delta\Gamma_s^{meas}$ with respect to the Standard Model expectation.

The mass eigenstates $|B_L\rangle$ (light) and $|B_H\rangle$ (heavy) at time $t = 0$ are defined as the linear combination of $|B_s\rangle$ and $|\bar{B}_s\rangle$:

$$|B_L\rangle = p|B_s\rangle + q|\bar{B}_s\rangle \quad (4)$$
$$|B_H\rangle = p|B_s\rangle - q|\bar{B}_s\rangle \quad (5)$$

with $|p|^2 + |q|^2 = 1$. Following the discussion in [5, 6] we introduce the following quantities:

$$\lambda_f = \frac{q}{p}\frac{\bar{A}_f}{A_f} = \eta_f e^{-i\Phi_M} \quad (6)$$

where $\Phi_M = \arg(M_{12})$, $A_f = \langle f|B_s\rangle$, $\bar{A}_f = \langle f|\bar{B}_s\rangle$ and η_f is the CP partity of $CP|f\rangle = \eta_f|f\rangle$. In addition:

$$A_{CP}^{dir} = \frac{1-|\lambda_f|^2}{1+|\lambda_f|^2} \qquad A_{CP}^{mix} = \frac{2Im(\lambda_f)}{1+|\lambda_f|^2} \qquad A_{\Delta\Gamma} = \frac{2Re(\lambda_f)}{1+|\lambda_f|^2} \quad (7)$$

which are related via $(A_{CP}^{dir})^2 + (A_{CP}^{mix})^2 + (A_{\Delta\Gamma})^2 = 1$. The general equation for the decay rate of the process $B_s \to f$ (with the general final state f) can be written as:

$$\Gamma[f,t] = \Gamma(B_s(t) \to f) + \Gamma(\bar{B}_s(t) \to f) \quad (8)$$
$$= N_f[e^{-\Gamma_L t}|\langle f|B_L\rangle|^2 + e^{-\Gamma_H t}|\langle f|B_H\rangle|^2] \quad (9)$$
$$\sim N_f|A_f|^2\left[1+|\lambda_f|^2\right]e^{-\Gamma t}\left\{\cosh\tfrac{\Delta\Gamma t}{2} + \sinh\tfrac{\Delta\Gamma t}{2}A_{\Delta\Gamma}\right\}. \quad (10)$$

Taking the overall normalisation such that $BR[all] = 1$, the overall normalisation N_f can be related to the branching ratio:

$$BR[f] = \frac{1}{2}\int_0^\infty dt\Gamma[f,t] \sim \frac{N_f}{2}|A_f|^2\left[1+|\lambda_f|^2\right]\frac{\Gamma + A_{\Delta\Gamma}\Delta\Gamma/2}{\Gamma^2 - (\Delta\Gamma/2)^2} \quad (11)$$

and hence:

$$\Gamma[f,t] = 2BR[f]\frac{\Gamma^2 - (\Delta\Gamma)^2}{\Gamma + A_{\Delta\Gamma}\Delta\Gamma/2}e^{-\Gamma t}\left\{\cosh\frac{\Delta\Gamma t}{2} + \sinh\frac{\Delta\Gamma t}{2}A_{\Delta\Gamma}\right\}. \quad (12)$$

This can be expressed as [6]:

$$\Gamma[f,t] = N_f\frac{|A_f|^2}{2}\left(1+|\lambda_f|^2\right)[(1-A_{\Delta\Gamma})e^{-\Gamma_L t} + (1+A_{\Delta\Gamma})e^{-\Gamma_H t}]. \quad (13)$$

The weak phase of the CKM suppressed $B_s^0 \to K^+K^-$ decay mode is not known as it is not yet understood how the penguin diagrams contribute with respect to the tree diagrams. However, using vertex counting it can be estimated that the $b \to u\bar{u}s$ tree diagram is suppressed. It is therefore expected that the dominant contribution arises from penguin diagrams and the contribution from Γ_H vanishes and hence this channel is mainly sensitive to Γ_L. Other channels such as $B_s^0 \to J/\psi\Phi$, $B_s^0 \to D_s^-\pi^+$ and $B_s^0 \to D_s^-\mu^+\nu_\mu$ allow a measurement of the double exponential distribution:

$$\Gamma[f,t] = Ae^{-\Gamma_L t} + Be^{-\Gamma_H t} = e^{-\Gamma t}\left[(A+B)\cosh\frac{\Delta\Gamma t}{2} + (B-A)\sinh\frac{\Delta\Gamma t}{2}\right] \quad (14)$$

and if this is fitted with a single exponential $\Gamma[f,t] = \Gamma_f e^{\Gamma_f t}$, the following result is obtained as shown in [7]:

$$\Gamma_f = \frac{A/\Gamma_L + B/\Gamma_H}{A/\Gamma_L^2 + B/\Gamma_H^2}. \quad (15)$$

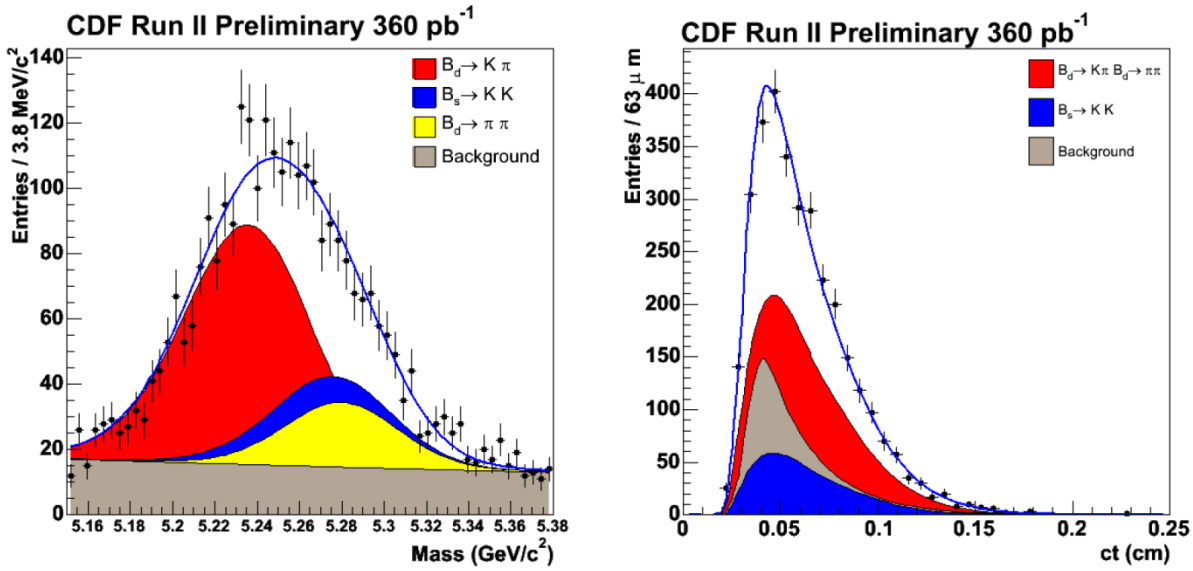

Figure 1 Projections of the combined mass and lifetime fit by CDF [8].

All of these measurements provide information on Γ_L and Γ_H with different correlations. For example in flavour specific decays, $A = B$ and and hence:

$$\tau_{fs} = \frac{\tau_L^2 + \tau_H^2}{\tau_L + \tau_H}. \tag{16}$$

If Γ_L and Γ_H are known, i.e. if τ_L is measured from $B_s^0 \to K^+K^-$ and τ_H is extracted numerically from (16) using the lifetime of the flavour-specific decays τ_{fs} as external input, the width difference $\Delta\Gamma$ can be calculated as:

$$\frac{\Delta\Gamma_{CP}}{\Gamma_{CP}} = 2\frac{\tau_H - \tau_L}{\tau_H + \tau_L}. \tag{17}$$

The uncertainty follows from error propagation:

$$\sigma\left(\frac{\Delta\Gamma_{CP}}{\Gamma_{CP}}\right) = 2\frac{\tau_{fs}}{\tau_L}\sqrt{\left(\frac{\sigma_{\tau_L}}{\tau_L}\right)^2 + \left(\frac{\sigma_{\tau_{fs}}}{\tau_{fs}}\right)^2}. \tag{18}$$

Exploiting the different correlation of the various measurements sensitive to $\Delta\Gamma/\Gamma$, both Γ_L and Γ_H can be extracted in a global fit to these measurements.

The corresponding results from a recent analysis by the CDF collaboration [8] are summarised below:

$$\tau(B_s^0 \to K^+K^-) = 1.53 \pm 0.18(\text{stat}) \pm 0.2(\text{syst}) \text{ ps}. \tag{19}$$

Using the HFAG average of the B_s^0 lifetime in flavour specific decays [9]: $\tau(B_sFS) = 1.454 \pm 0.040$ ps, the measured lifetime is translated into:

$$\frac{\Delta\Gamma_{CP}}{\Gamma_{CP}}(B_s^0 \to K^+K^-) = -0.08 \pm 0.23 \pm 0.03. \tag{20}$$

Figure 1 shows the mass and lifetime projections of the unbinned likelihood fit from the CDF result.

1.2 LHCb Monte Carlo simulation data samples

The LHCb Monte Carlo simulation uses the Pythia event generator [10] to simulate the underlying physics event, decays and radiative effects are handled by EvtGen [11] and PHOTOS [12] and these are run through a full GEANT4 [13] detector simulation. The events were reconstructed and analysed using the LHCb software packages Brunel v35r2 and DaVinci v23r3p1. We use a sample of 680,000 B hadron decays to charged hadrons ($H_b \to h^+h'^-$) including 50,000 $B_s^0 \to K^+K^-$ and 50,000 $B_d^0 \to K^+\pi^-$ events.

2 Measuring the $B_s \to KK$ lifetime

2.1 Overview

This analysis is designed to make an unbiased measurement of the $B_s^0 \to K^+K^-$ lifetime. Since most combinatorial background originates at the primary vertex we select tracks that are significantly displaced from the primary vertex in order to obtain a clean sample of B hadrons. Such selections are present in both the trigger of the LHCb experiment and offline.

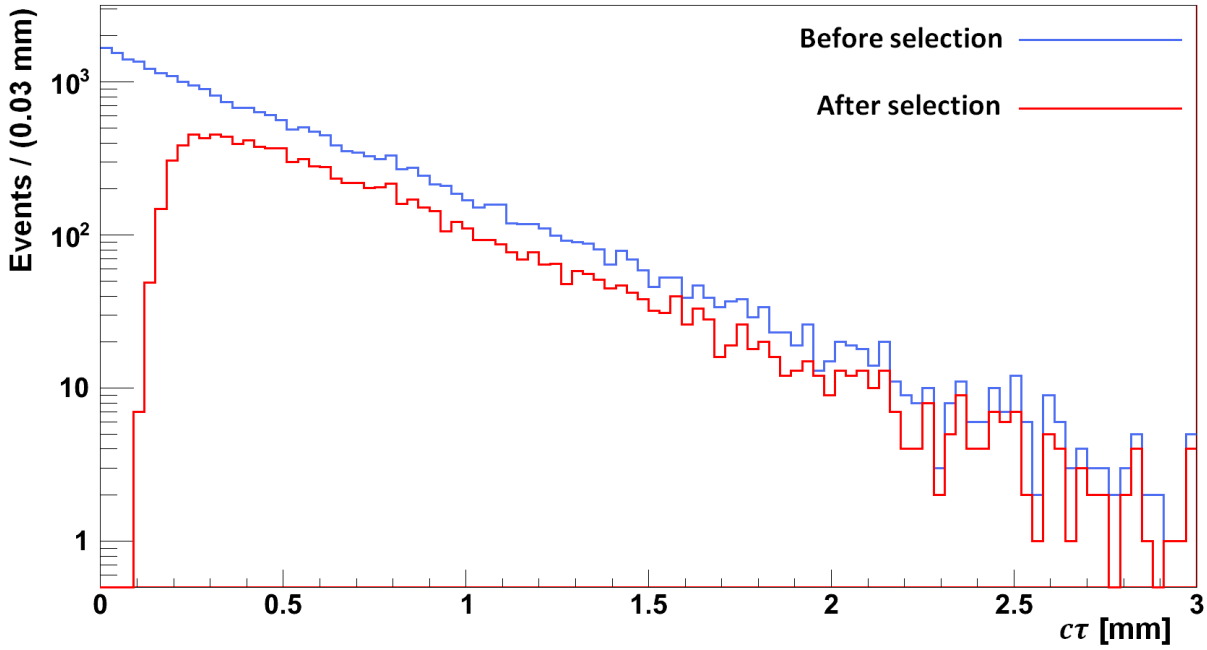

Figure 2 The distribution of the true proper lifetime of B_s^0 mesons from simulated $B_s^0 \to K^+K^-$ decays before and after offline selection cuts.

However, these selections tend to reject particles with short proper lifetimes which decay closer to the primary vertex. As a result, the proper lifetime distributions of particles collected using such a selection are biased to longer lifetime. In Figure 2 we see the effect of the offline selection on the true proper lifetime distribution of B_s^0 mesons from simulation. We see that the proper lifetime distribution is truncated at low values leading to a distortion of the distribution.

Methods have been developed by the authors of [14] and [15] which correct for this bias by calculating an event by event acceptance function from the decay geometry without relying on Monte Carlo simulation. Another approach has been devised in [16] which avoids the use of lifetime-biasing impact parameter selections by using a particle identification based selection to remove combinatorial backgrounds. Here we present a different approach based on eliminating

bias through comparison of topologically related B decays which will be able to provide an early result at LHC*b*.

We will measure the $B_s^0 \to K^+K^-$ lifetime by comparing the proper lifetime distribution with that of the decay mode $B_d^0 \to K^+\pi^-$. Since these channels share the same topology and have very similar kinematic distributions we expect the lifetime biasing effect of the selection to be the same for each. By taking a ratio of their respective proper lifetime distributions we will cancel selection bias along with many other systematic effects.

We isolate the two channels' proper lifetime distributions by performing a series of un-binned maximum likelihood fits to the invariant mass distribution in bins of proper lifetime/mass. From these fits we extract the yield of each decay in bins of proper lifetime, produce a plot of the ratio of the yields of $B_s^0 \to K^+K^-$ to $B_d^0 \to K^+\pi^-$ and thus extract the $B_s^0 \to K^+K^-$ lifetime using the measurement of the mean B_d^0 lifetime from CDF and the B-factories [17].

This method has the advantage of requiring relatively low statistics to produce a measurement. It may also be used early in the experimental run when the performance of the detector has not been fully characterised, since we expect almost all lifetime-biasing effects to be the same for each channel and therefore be cancelled in the ratio.

In principle this approach may also be used to measure the lifetime of any decay mode where a suitable reference channel exists. For example, we could apply this method to measure the mean B_s^0 lifetime through the decay mode $B_s^0 \to \pi^+K^-$. However, due to a smaller branching ratio we expect lower statistics from this channel than for $B_s^0 \to K^+K^-$. It is also possible to measure the lifetime of the Λ_b^0 baryon from the decay modes $\Lambda_b^0 \to p^+K^-$ and $\Lambda_b^0 \to p^+\pi^-$. However, in these cases systematic effects may be cancelled less completely since no reference channel with the same topology exists in our mass window.

2.2 Event selection

In order to extract the signals of interest we must reject both *physical* and *combinatorial* backgrounds. Physical backgrounds are particle decays which yield an invariant mass in the same region as our signals of interest. Combinatorial backgrounds arise from the reconstruction of B hadron candidates from unrelated, oppositely charged tracks.

There are two physical backgrounds which we aim to reduce. The first are the partially reconstructed three-body decays such as $B_s^0 \to \rho^+(\pi^+\pi^0)K^-$. These decays give reconstructed masses below around 5.2 GeV/c^2 and their mass distributions overlap most strongly with the low mass tails of the two-body B hadron decays. The second physical background includes all two-body B hadron decays other than our signals of interest. The most problematic of these channels is $B_d^0 \to \pi^+\pi^-$ which gives a mass distribution that overlaps very strongly with that of $B_s^0 \to K^+K^-$. In order to extract our signal at low integrated luminosity we will need to reject as much of these backgrounds as possible.

Our selection is based upon the standard $H_b \to h^+h'^-$ selection presented in [18] and described in detail in [19]. The $H_b \to h^+h'^-$ offline selection criteria are presented in Table 1. Figure 4 shows the distributions of the $H_b \to h^+h'^-$ selection variables for true $B_s^0 \to K^+K^-$ candidates and combinatorial background from signal events.

In addition to the standard $H_b \to h^+h'^-$ selection we impose a cut on the RICH particle identification (PID) [1,20] in order to reduce the $B_d^0 \to \pi^+\pi^-$ signal:

$$max\left[(\Delta \ln \mathcal{L}_{K\pi})^h, (\Delta \ln \mathcal{L}_{K\pi})^{h'}\right] > 10 \qquad (21)$$

where $\mathcal{L}_{K\pi}$ is the likelihood for the daughter to be a kaon relative to the pion hypothesis. The efficiency of this cut for each decay mode along with the total selection efficiency and anticipated yield is presented in Table 2 [18]. Table 3 shows the correlations of all the offline selection variables.

Selection criteria	Accepted region
$min\left[(IP/\sigma_{IP})^h, (IP/\sigma_{IP})^{h'}\right]$	> 6
$max\left[(IP/\sigma_{IP})^h, (IP/\sigma_{IP})^{h'}\right]$	> 12
$min\left(p_T^h, p_T^{h'}\right)$ [GeV/c]	> 1
$max\left(p_T^h, p_T^{h'}\right)$ [GeV/c]	> 3
m [GeV/c^2]	[5.0 , 5.8]
p_{T_B} [GeV/c]	> 1.0
L_B/σ_{L_B}	> 18
IP_B/σ_{IP_B}	< 2.5
χ^2	< 5

Table 1 The standard $H_b \to h^+h'^-$ offline selection criteria [18]. IP is the impact parameter with respect to the primary vertex, p_T is the transverse momentum, m is the invariant mass of the B candidate, L_B is the distance of flight of the B candidate and χ^2 is the χ^2 statistic of the vertex fit. σ refers to the standard error on a quantity and the labels h, h' and B refer to the two daughters and the B candidate respectively.

Channel	f_{hadr} [%]	BR × 10^{-6}	ϵ_{sel} [%]	$\epsilon_{\mathcal{L}/sel}$ [%]	$\epsilon_{trig/sel}$ [%]	ϵ_{tot} [%]	Yield / fb^{-1}
$B_s^0 \to K^+K^-$	10.1 ± 0.9	26 ± 4	3.69 ± 0.05	84.0 ± 1.5	37.4 ± 0.5	1.16 ± 0.03	30,500
$B_s^0 \to \pi^+K^-$	10.1 ± 0.9	5.3 ± 1.2	3.83 ± 0.07	62.2 ± 1.2	37.0 ± 1.0	0.88 ± 0.03	4,700
$B_d^0 \to K^+\pi^-$	40.3 ± 0.9	19.4 ± 0.6	3.84 ± 0.04	64.4 ± 1.2	36.1 ± 0.3	0.89 ± 0.02	69,600
$B_d^0 \to \pi^+\pi^-$	40.3 ± 0.9	5.2 ± 0.2	3.95 ± 0.05	1.2 ± 0.3	35.8 ± 0.6	0.02 ± 0.01	400
$\Lambda_b^0 \to p^+K^-$	9.2 ± 1.5	5.0 ± 1.2	3.32 ± 0.05	76 ± 2	35.7 ± 0.7	0.90 ± 0.03	4,100
$\Lambda_b^0 \to p^+\pi^-$	9.2 ± 1.5	3.1 ± 0.9	3.36 ± 0.06	31.5 ± 1.1	36.8 ± 1.1	0.39 ±0.02	1,100

Table 2 Selection efficiencies and anticipated yields for the $H_b \to h^+h'^-$ decay modes. f_{hadr} is the fraction of b quarks that hadronise to the B hadron initial state, ϵ_{sel} is the efficiency for the standard $H_b \to h^+h'^-$ selection and includes the efficiency of due to detector angular acceptance, $\epsilon_{\mathcal{L}/sel}$ is the efficiency of the RICH PID selection for candidates passing the $H_b \to h^+h'^-$ selection, $\epsilon_{trig/sel}$ is the efficiency of the trigger for candidates passing the $H_b \to h^+h'^-$ selection and ϵ_{tot} is the total efficiency of the selection. The yield is calculated given a $b\bar{b}$ production cross-section of $\sigma_{b\bar{b}} = 500\,\mu$b. The yield per fb^{-1} for a particular decay mode is given by $Y = \sigma_{b\bar{b}} \cdot 2 \cdot f_{hadr} \cdot BR \cdot \epsilon_{tot}$ where the factor of two comes from the fact that the b quarks are produced in pairs.

We can see that the $\Delta \ln \mathcal{L}_{K\pi}$ selection successfully reduces the $B_d^0 \to \pi^+\pi^-$ yield to around 1% of the $B_s^0 \to K^+K^-$ yield. However, this selection will not affect the decays $B_s^0 \to K^+K^-$ and $B_d^0 \to K^+\pi^-$ in the same way since they have different $\Delta \ln \mathcal{L}_{K\pi}$ distributions. As a result taking a ratio of proper lifetime distributions of these two decay modes will not necessarily remove lifetime bias introduced by this selection. It is therefore important to understand whether this selection affects a lifetime measurement. Figure 3 shows a plot of the ratio of the acceptance

functions for $B_s^0 \to K^+K^-$ and $B_d^0 \to K^+\pi^-$ for the $\Delta \ln \mathcal{L}_{K\pi}$ selection as function of proper lifetime. This distribution has been fitted with a straight line and we see that the gradient is consistent with zero to within statistical precision. This indicates that the use of this PID selection will not bias our lifetime measurement as the ratio of the acceptance functions for our two signal decays does not vary with proper lifetime.

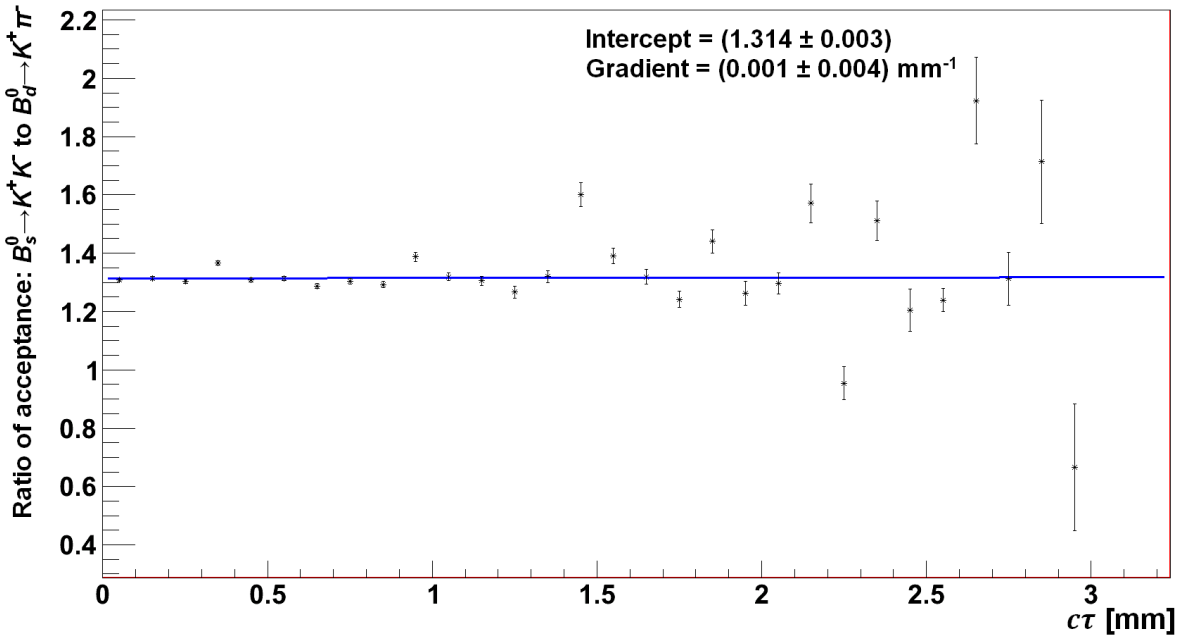

Figure 3 The ratio of the acceptance of the $\Delta \ln \mathcal{L}_{K\pi}$ selection (21) as a function of proper lifetime, $c\tau$, with a first order polynomial fit. This plot was produced using true $B_s^0 \to K^+K^-$ and $B_d^0 \to K^+\pi^-$ candidates from the full LHC*b* Monte Carlo simulation datasets described in 1.2.

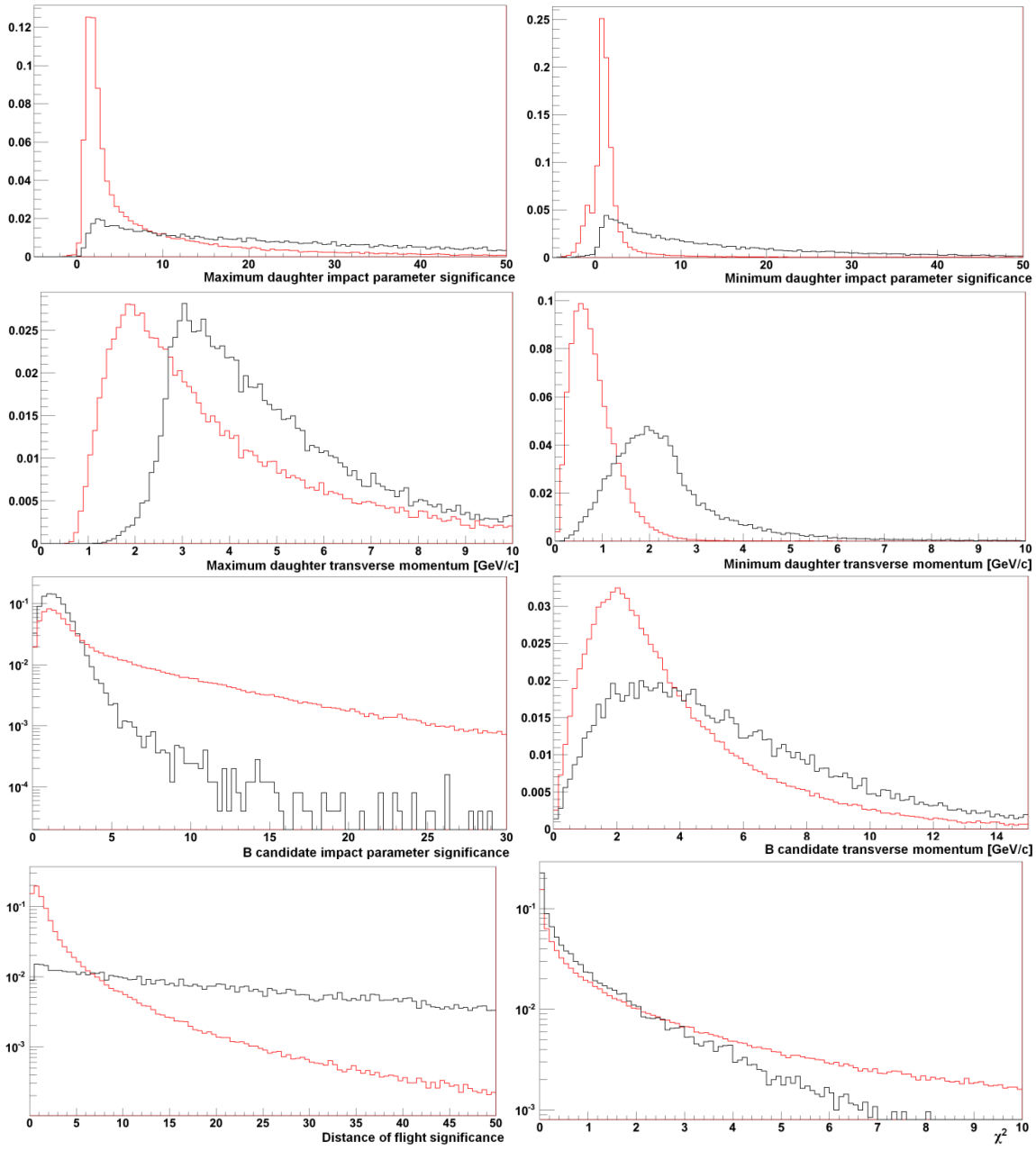

Figure 4 $H_b \to h^+h'^-$ selection variables for true $B_s^0 \to K^+K^-$ candidates (black) and combinatorial background from signal events (red).

	$max(p_T^h, p_T^{h'})$ [GeV/c]	$min(p_T^h, p_T^{h'})$ [GeV/c]	p_{T_B}[GeV/c]	$max[(IP/\sigma_{IP})^h, (IP/\sigma_{IP})^{h'}]$	$min[(IP/\sigma_{IP})^h, (IP/\sigma_{IP})^{h'}]$	IP_B/σ_{IP_B}	L_B/σ_{L_B}	χ^2	m [GeV/c^2]	$max[(\Delta \ln \mathcal{L}_{K\pi})^h, (\Delta \ln \mathcal{L}_{K\pi})^{h'}]$
$max(p_T^h, p_T^{h'})$ [GeV/c]		0.279	0.912	0.040	0.081	−0.020	0.065	−0.020	−0.083	−0.246
$min(p_T^h, p_T^{h'})$ [GeV/c]			0.551	0.022	0.192	−0.024	0.064	−0.023	0.229	−0.141
p_{T_B}[GeV/c]				0.054	0.106	−0.017	0.079	−0.018	−0.045	−0.256
$max[(IP/\sigma_{IP})^h, (IP/\sigma_{IP})^{h'}]$					0.723	0.042	0.927	−0.005	−0.043	−0.018
$min[(IP/\sigma_{IP})^h, (IP/\sigma_{IP})^{h'}]$						0.037	0.818	−0.006	0.131	0.003
IP_B/σ_{IP_B}							0.030	0.118	−0.229	0.005
L_B/σ_{L_B}								−0.016	−0.014	0.001
χ^2									−0.018	−0.022
m [GeV/c^2]										0.105
$max[(\Delta \ln \mathcal{L}_{K\pi})^h, (\Delta \ln \mathcal{L}_{K\pi})^{h'}]$										

Table 3 Correlations of the offline selection variables for true $B_s^0 \to K^+K^-$ candidates.

2.3 Mass fit

The yield of each channel for each proper lifetime bin is extracted using a fit to the invariant mass distribution in the range 5.0 – 5.8 GeV/c^2. Events are reconstructed as two-body decays with a pion mass hypothesis for the daughters. Currently we fit for the following two-body decay channels (and their charge conjugates):

- $B_s^0 \to K^+K^-$
- $B_s^0 \to \pi^+K^-$
- $B_d^0 \to K^+\pi^-$
- $B_d^0 \to \pi^+\pi^-$
- $\Lambda_b^0 \to p^+K^-$
- $\Lambda_b^0 \to p^+\pi^-$

and for the partially reconstructed three-body decay $B_s^0 \to \rho^+(\pi^+\pi^0)K^-$.

As the fit progresses it will be necessary to fit for all possible three-body decays; for example $B \to \rho K$, $B \to K^*\pi$ and $B \to \rho K$. It may also be necessary to fit for the two-body decay modes $B_d^0 \to K^+K^-$ and $B_s^0 \to \pi^+\pi^-$ though these are expected to have very small branching fractions.

2.3.1 Invariant mass line shapes

If we are to reliably extract the yield of each decay mode it is essential to develop probability distribution functions (PDFs) which accurately model their invariant mass distributions. The form of these distributions should include the effects of experimental resolution, energy loss through QED radiative processes and the use of incorrect mass hypotheses for the daughter particles.

The effect of detector resolution is to broaden the invariant mass lineshape from a very narrow Breit-Wigner distribution to a much broader Gaussian. The Breit-Wigner distribution may be treated as a delta function positioned at the B hadron mass since its width is much narrower than detector resolution. The convolution of the Gaussian resolution function with the original Breit-Wigner is therefore simply the same Gaussian with mean equal to the B hadron mass.

QED radiative processes also alter the invariant mass lineshapes. As the charged daughter particles from the decay of a B hadron travel through the detector they lose energy through bremsstrahlung. As a result, their measured momenta are lower than their initial momenta. This leads to an underestimation of the original B hadron mass, introducing a low mass tail to the distribution.

The mass of the B hadron is calculated as the invariant mass of the charged final state particles. For the decay $H_b \to h^+h'^-$ the B mass is given by:

$$m_B^2 = m_+^2 + m_-^2 + 2\sqrt{(\vec{p}_+^{\,2} + m_+^2)(\vec{p}_-^{\,2} + m_-^2)}. \tag{22}$$

When calculating the B hadron mass we assume the pion mass, $m_\pi = 139.6$ MeV/c², for the masses of the daughter particles, m_+ and m_-. In the event that the daughter was actually a kaon ($m_K = 493.7$ MeV/c²) or proton ($m_P = 938.3$ MeV/c²) this will lead to an underestimation of the B hadron mass. This misassignment shifts the mean of the invariant mass distributions of all decay modes other than $B_d^0 \to \pi^+\pi^-$ to lower values and also skews the distributions leading to longer low mass tails.

To model these effects each channel, including three-body decays, is fitted with the same form of invariant mass PDF:

$$P(m) = f \times CB(m; \bar{m}_1, \sigma_1, \alpha, n) + (1-f) \times G(m; \bar{m}_1, \sigma_2) \tag{23}$$

where $G(m; \bar{m}_1, \sigma_2)$ is a Gaussian distribution (with mean $\bar{m}_1$, standard deviation σ_2), CB is a Crystal Ball distribution [21], a piecewise distribution composing a central Gaussian with low mass tail, where:

$$CB(m; \bar{m}_1, \sigma_1, \alpha, n) = \begin{cases} e^{-(m-\bar{m}_1)^2/2\sigma_1^2} & \dfrac{m-\bar{m}_1}{\sigma} > -\alpha \\ A\left(B - \dfrac{m-\bar{m}_1}{\sigma_1}\right)^{-n} & \dfrac{m-\bar{m}_1}{\sigma} \le -\alpha \end{cases} \tag{24}$$

with:

$$A = \left(\frac{n}{|\alpha|}\right)^n e^{-\alpha^2/2} \qquad B = \frac{n}{|\alpha|} - |\alpha| \tag{25}$$

and f is the fraction of the area of the PDF under the Crystal Ball distribution. The Gaussian distribution is included to model the effect of detector resolution. The Crystal Ball distribution models the low mass tail caused by both the incorrect mass hypotheses and QED radiative processes. These PDFs are implemented in RooFit [22] which automatically normalises the distributions to the number of events in the dataset being fitted.

This choice of PDF fits all channels very effectively as shown by Figure 5 where we see the results of the fit to the invariant mass distributions of each channel. The shape of the three-body, partially reconstructed invariant mass distribution is not yet well understood due to low Monte Carlo statistics. At present we fit these decays with the same PDF as shown above, however an Argus function convoluted with a Gaussian has also been suggested as an alternative. This may be difficult to implement practically due to the high computational demand of a convolution.

A detailed discussion of the parameterization of the $H_b \to h^+h'^-$ invariant mass distributions is presented in [18]. The authors have designed PDFs which model the effects of detector resolution, QED radiative processes, mass dependent acceptance and incorrect mass hypotheses in a theoretically rigorous fashion.

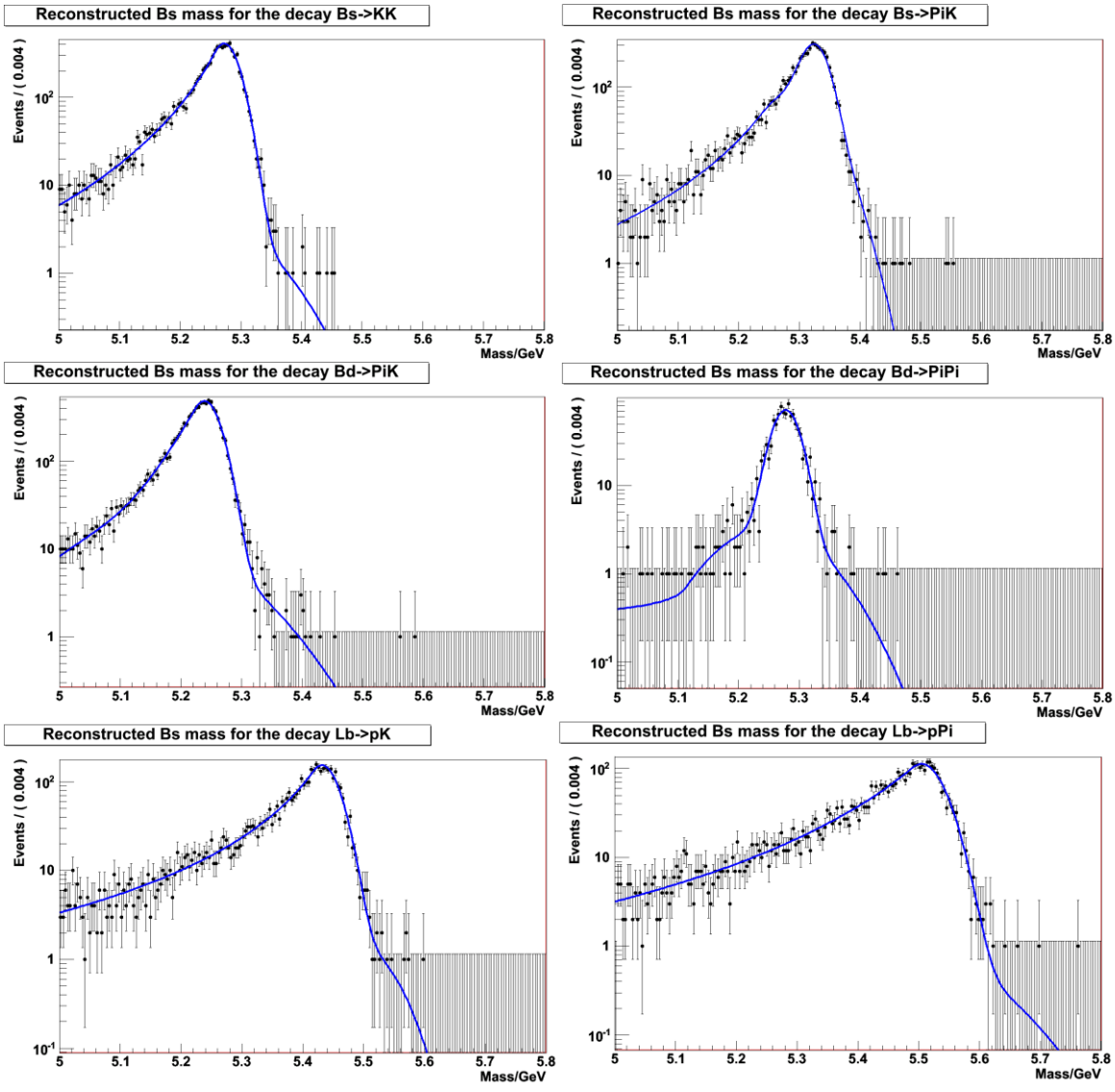

Figure 5 Fits to the invariant mass distributions of $B_s^0 \to K^+K^-$, $B_s^0 \to K^-\pi^+$, $B_d^0 \to K^+\pi^-$, $B_d^0 \to \pi^+\pi^-$, $\Lambda_b^0 \to K^-p^+$ and $\Lambda_b^0 \to \pi^-p^+$.

However, in practice these PDFs, while producing excellent agreement between simulation and fit parameters, are computationally demanding and have been deemed unsuitable for high statistics toy studies. Therefore we have adopted the simplified model described above for the purposes of this study.

2.3.2 Fit to the complete invariant mass distribution

The PDF used to fit the complete invariant mass distribution is essentially a sum of the single channel invariant mass PDFs. First we construct a PDF for each hadron type (B_s^0, B_d^0, Λ_b^0):

$$PDF_{B_s}(m) = f_{B_sKK} P_{B_sKK}(m) + f_{B_s\pi K} P_{B_s\pi K}(m) + (1 - f_{B_sKK} - f_{B_s\pi K}) P_{B_s\rho K}(m), \quad (26)$$

$$PDF_{B_d}(m) = f_{B_d\pi K} P_{B_d\pi K}(m) + (1 - f_{B_d\pi K}) P_{B_d\pi\pi}(m) \quad (27)$$

and

$$PDF_{\Lambda_b}(m) = f_{\Lambda_b pK} P_{\Lambda_b pK}(m) + (1 - f_{\Lambda_b pK}) P_{\Lambda_b p\pi}(m) \quad (28)$$

where f are fraction coefficients and P are the single channel PDFs discussed in 2.3.1. The overall fitting function is then:

$$PDF_{Total}(m) = N_{B_s} PDF_{B_s}(m) + N_{B_d} PDF_{B_d}(m) + N_{\Lambda_b} PDF_{\Lambda_b}(m) \quad (29)$$

where N are the yields for each particle. This PDF uses the extended likelihood formalism where we not only fit for the relative proportions of the numbers of different particles but also for the total number of candidates.

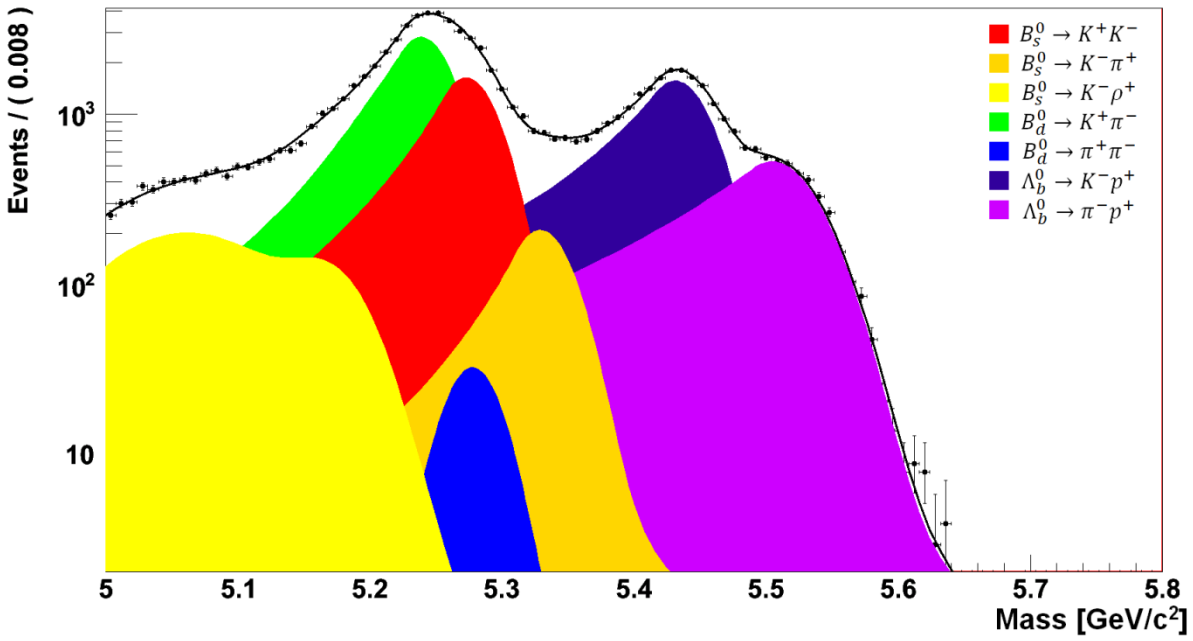

Figure 6 A fit to the full $H_b \to h^+h'^-$ invariant mass spectrum.

This final fitting function has a total of 49 parameters. However, once the single channel shapes have been fitted to true simulated events their parameters are fixed and we fit only for the yields of each channel leaving us with seven free parameters. This makes for a fast fitting process but requires a good correspondence between Monte Carlo simulation and data. An example of the fit to the full invariant mass distribution is shown in Figure 6.

At present we do not fit for combinatorial background since the selection almost completely removes it from the available Monte Carlo datasets. We require larger amounts of full LHC*b* simulated data in order to perform a detailed background study. This should be available with the 2009 generation of simulated data. We will also fit for additional three-body decays when larger simulated statistics are available.

2.3.3 Implementation

The fit is implemented in RooFit [22], a ROOT [23] toolkit for modelling the expected distributions of events in a physics analysis. The likelihood statistic is calculated by RooFit and the statistic minimized by MINUIT [24] implemented in ROOT. MINUIT also calculates asymmetric errors on the fitting parameters through the MINOS method.

2.4 Lifetime extraction

The proper lifetime of a *B* candidate is calculated as

$$c\tau = L_{3D}\frac{m}{|\vec{p}|} \tag{30}$$

where m is the calculated mass of the candidate, L_{3D} is the three dimensional flight distance of the particle and $\vec{p}$ is its three-momentum in the lab frame. Since we assume a pion mass hypothesis for the daughters in all decay channels the proper lifetime distributions are biased for all $H_b \to h^+h'^-$ channels other than $B_d^0 \to \pi^+\pi^-$. In order to avoid biasing the measured $B_s^0 \to K^+K^-$ lifetime we therefore work with the mass independent quantity

$$\xi = \frac{\tau}{m} = \frac{L_{3D}}{|\vec{p}|}. \tag{31}$$

The invariant mass fit described above is performed for six bins of ξ. The bin edges are chosen such that the number of $B_s^0 \to K^+K^-$candidates per bin is approximately constant. These bin edges are given in Table 4.

Bin	Lower edge / mmGeV^{-1}	Upper edge / mmGeV^{-1}
1	0.0000	0.0516
2	0.0516	0.0726
3	0.0726	0.0966
4	0.0966	0.1296
5	0.1296	0.1830
6	0.1830	0.6000

Table 4 cξ bin edges given in terms of proper lifetime multiplied by the speed of light dividied by mass.

Ideally, we would like to have as many bins in ξ as possible in order to produce a more accurate fit for the $B_s^0 \to K^+K^-$ lifetime. However, increasing the number of bins reduces the number of events in each bin and so reduces the precision of our invariant mass fit. The optimum number of bins will also depend upon the number of events being fitted for and on the background present in real data. Hence early in data taking a smaller number of bins may be required compared to when we have larger statistics.

The yields of $B_s^0 \to K^+K^-$ and $B_d^0 \to K^+\pi^-$ are extracted from each fit and plotted as a function of ξ. This reproduces a binned proper lifetime/mass distribution for each channel. The measured ξ distribution for a particular channel is of the form:

$$F_{meas}(\xi) = [F_{true}(\xi) * G_{res}(\xi)] \times H_{acc}(\xi). \tag{32}$$

$F_{true}(\xi)$ is the true proper lifetime/mass distribution for the channel and is equal to:

$$F_{true}(\xi) = \begin{cases} Ae^{-tm_{true}/\tau m_{meas}} & t \geq 0 \\ 0 & \text{otherwise} \end{cases} \tag{33}$$

where A is a constant, t is the measured proper lifetime, τ is the mean lifetime of the decay mode, m_{true} is the true mass of the candidate and m_{meas} is the measured mass of the candidate. This is convolved with a Gaussian resolution function:

$$G_{res}(\xi) = e^{-\xi^2/2\sigma^2} \tag{34}$$

where σ is the detector resolution. $H_{acc}(\xi)$ is the acceptance function which is the probability that a candidate with proper lifetime/mass ξ is passed by the trigger, online and offline cuts. It is this function which biases our proper lifetime distribution to longer lifetime.

Since $B_s^0 \to K^+K^-$ and $B_d^0 \to K^+\pi^-$ have the same topology we expect that $H_{acc}(\xi)$ will be the equal (to within a multiplicative constant) for each channel. Violations of this equality may, however, occur, for example, as a result of a slight difference in opening angle due to the different masses of the daughters for each channel. Figure 7 shows a plot of the ratio of the acceptance functions for the offline selection in Section 2.2 for full LHC*b* simulated events.

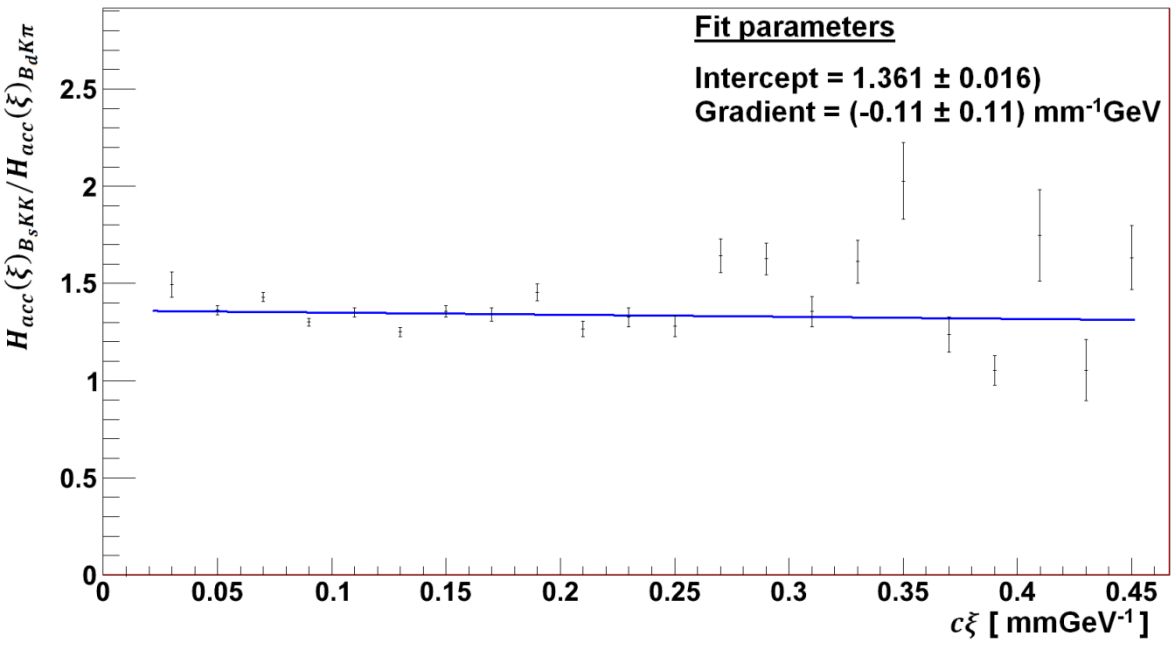

Figure 7 Plot of the ratio of the acceptance functions of the offline cuts for the channels $B_s^0 \to K^+K^-$ and $B_d^0 \to K^+\pi^-$.

A straight line fit to this ratio is consistent with being flat. We can conclude, therefore, that our assumption that the acceptance functions are equal for each channel is justified and so the ratio of their proper lifetime distributions will be:

$$R(\xi) = B\frac{F_{true}\left(\xi, \tau_{B_s \to KK}/m_s\right) * G_{res}(\xi, \sigma)}{F_{true}(\xi, \tau_d/m_d) * G_{res}(\xi, \sigma)} \tag{35}$$

where B is a constant. This ratio cancels the lifetime biasing term and allows us to make an unbiased measurement of the $B_s^0 \to K^+K^-$ lifetime. The ratio may be expressed as:

$$R(\xi) = B\frac{\int_0^\infty Ae^{-\xi' m_s/\tau_{B_s \to KK}} e^{-(\xi'-\xi)^2/2\sigma^2} d\xi'}{\int_0^\infty Ae^{-\xi' m_d/\tau_d} e^{-(\xi'-\xi)^2/2\sigma^2} d\xi'} \tag{36}$$

which is not calculable analytically but to a good approximation the Gaussian resolution functions cancel and the ratio is equal to:

$$R(\xi) = Be^{-\xi\left(\frac{m_s}{\tau_{B_s \to KK}} - \frac{m_d}{\tau_d}\right)}. \tag{37}$$

We plot the natural log of this ratio against the mean value of the proper lifetime for each bin and fit for the gradient which is equal to:

$$g = -\left(\frac{m_s}{\tau_{B_s \to KK}} - \frac{m_d}{\tau_d}\right). \tag{38}$$

We can then extract our value for the $B_s^0 \to K^+K^-$ lifetime using the better constrained value of the mean B_d^0 lifetime ($\tau_d = (1.530 \pm 0.009)$ps) and the well measured B_s^0 and B_d^0 masses ($m_s = (5.3663 \pm 0.0006)$GeV, $m_d = (5.2795 \pm 0.0003)$GeV) [17].

3 Toy Monte Carlo simulation studies

In this section we describe a simple toy model that we use to test the efficacy of the analysis, check for bias and also to understand what level of precision we can achieve with a given quantity of data.

3.1 Toy model

The toy model is composed of two parts; each channel is given an invariant mass distribution and a proper lifetime distribution. The invariant mass distributions are the same as those described in 2.3.1 with the parameters of each distribution taken from fits to true candidates of each type from Monte Carlo data. The proper lifetime distributions are convolutions of a decaying exponential with a Gaussian resolution function:

$$PDF_t(t) = \int_0^\infty e^{-t'/\tau} e^{-(t'-t)^2/2\sigma^2} dt' \tag{39}$$

where t is proper lifetime and τ is the particle lifetime. The experimental resolution, σ, is set at 0.014 mm in agreement with the full Monte Carlo simulation. The values of τ used are given in Table 5. The total PDF for each channel is then simply:

$$PDF(m,t) = PDF_t(t) \cdot PDF_m(m) \tag{40}$$

Examples of generated data along with the PDFs are shown in Figure 8 and Figure 9. The relative number of candidates for each channel that is generated for a toy is set by the branching ratio and the cut efficiencies for that channel.

Decay mode	τ / ps	$c\tau$ / mm
$B_s^0 \to K^+K^-$	1.4707	0.4409
$B_d^0 \to K^+\pi^-$	1.5301	0.4578
$\Lambda_b^0 \to p^+K^-$	1.3840	0.4149

Table 5 The lifetimes for each particle used in Toy Monte Carlo generation.

It should be made explicit that this toy model does not attempt to check the success of the ratio method in cancelling lifetime bias introduced by impact parameter based selections. The purpose of this model is simply to check the effectiveness of extracting proper lifetime distributions by use of mass fits in bins of proper lifetime and to make sure that this essential element of the analysis does not itself introduce bias. A more sophisticated toy model that includes lifetime biasing selections will be developed in the future.

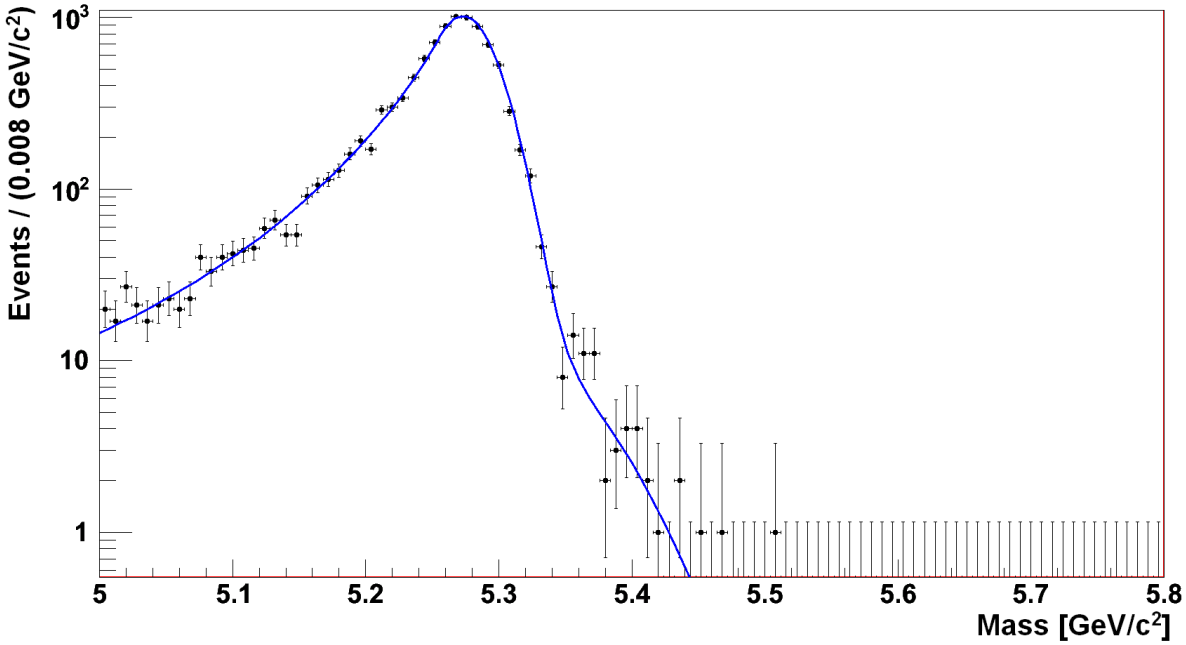

Figure 8 Toy Monte Carlo invariant mass data and PDF for 10,000 $B_s^0 \to K^+K^-$ candidates.

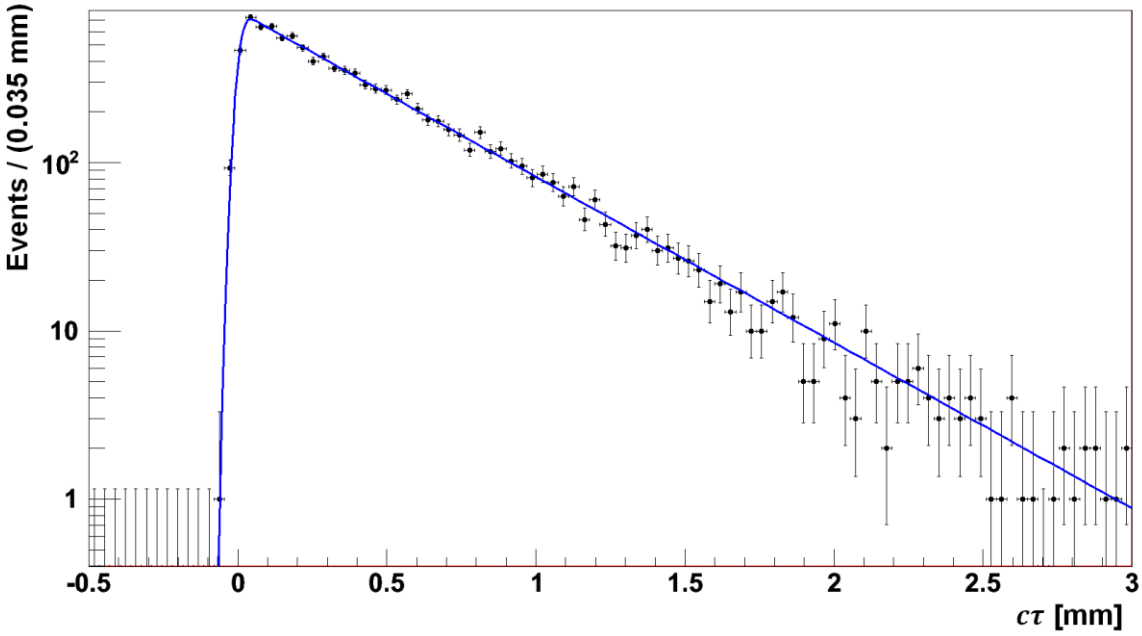

Figure 9 Toy Monte Carlo proper lifetime data and PDF for 10,000 $B_s^0 \to K^+K^-$ candidates.

3.2 Results of the standard analysis

We generated 3,000 datasets from the toy model described in 3.1. Each dataset contained the full range of $H_b \to h^+h'^-$ decay modes. The numbers of candidates generated for each channel in each dataset are listed in Table 6. The analysis described in Section 1 was then run on each dataset and the measured $B_s^0 \to K^+K^-$ and $\Lambda_b^0 \to p^+K^-$ lifetimes recorded (where the $\Lambda_b^0 \to p^+K^-$ lifetime is measured in the same way as the $B_s^0 \to K^+K^-$ lifetime). The results of these studies are presented below in Table 7, Figure 10, Figure 11, Figure 12 and Figure 13.

Channel	Number of candidates generated
$B_s^0 \to K^+K^-$	10,000
$B_s^0 \to K^-\pi^+$	1,541
$B_s^0 \to K^-\rho^+$	300
$B_d^0 \to K^+\pi^-$	22,820
$B_d^0 \to \pi^+\pi^-$	131
$\Lambda_b^0 \to K^-p^+$	1,344
$\Lambda_b^0 \to \pi^-p^+$	361

Table 6 The number of candidates for each channel generated for each toy Monte Carlo study.

Decay mode	Input Lifetime / ps	Mean Measured Lifetime / ps
$B_s^0 \to K^+K^-$	1.4707	1.4716 ± 0.0009
$\Lambda_b^0 \to p^+K^-$	1.3840	1.3864 ± 0.0012

Table 7 The mean measured lifetimes from 3,000 toy Monte Carlo studies.

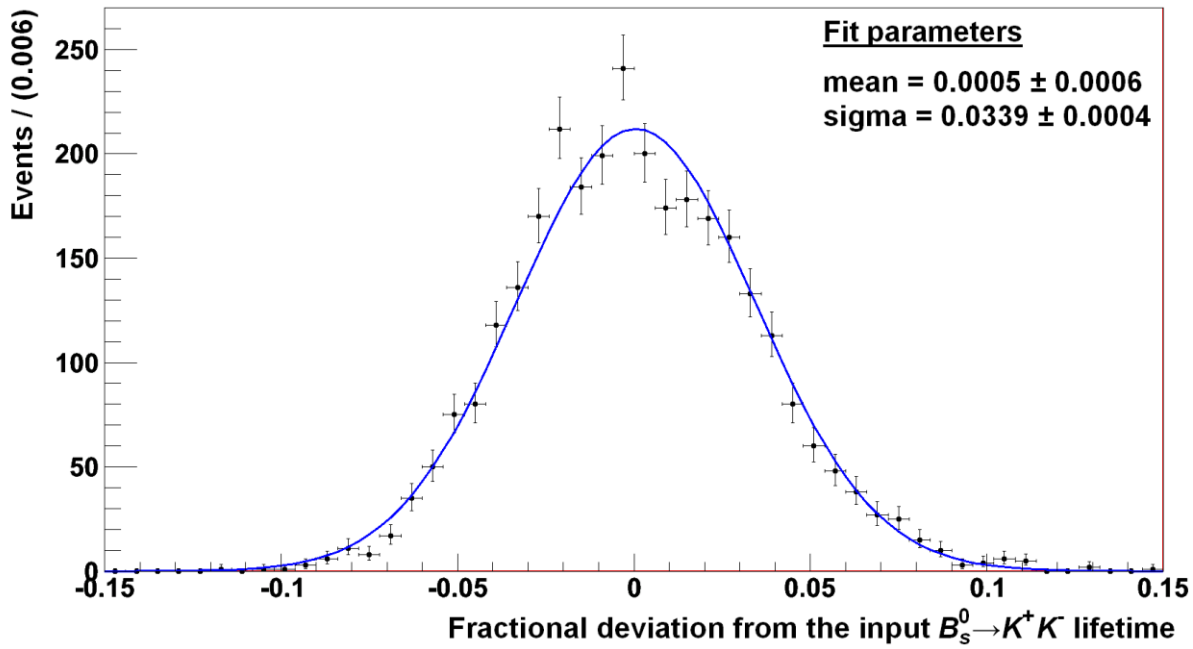

Figure 10 Distribution of the fractional deviations from the input $B_s^0 \to K^+K^-$ lifetime for 3,000 toy studies fitted with a Gaussian distribution.

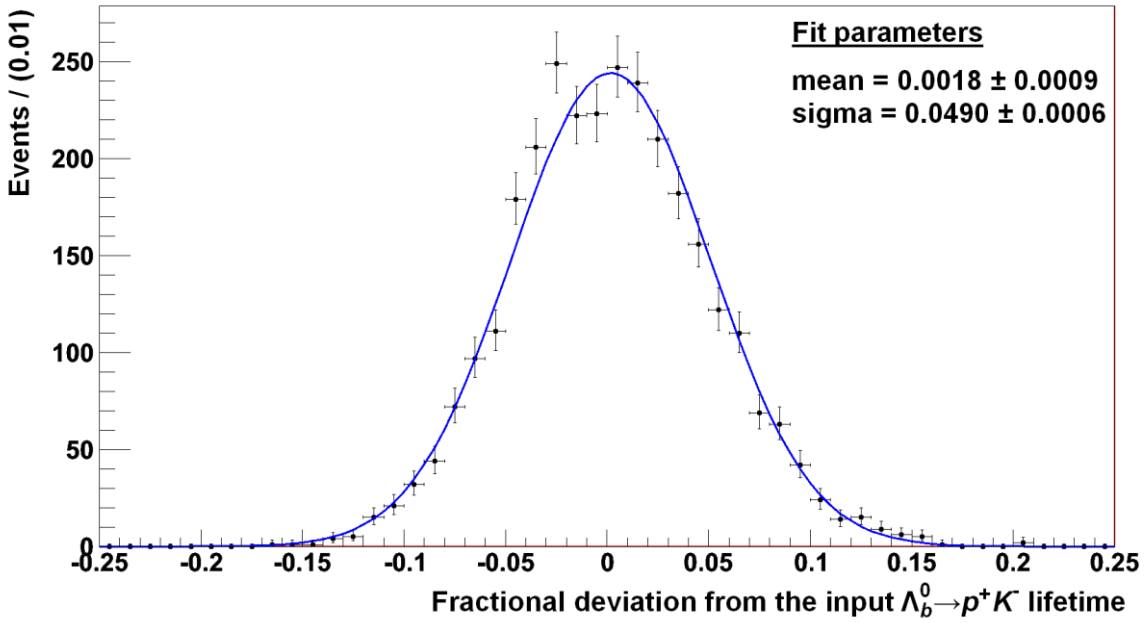

Figure 11 Distribution of the fractional deviations from the true $\Lambda_b^0 \to p^+K^-$ lifetime for 3,000 toy studies fitted with a Gaussian distribution.

From Table 7 and Figure 10 we see that the $B_s^0 \to K^+K^-$ lifetime measured by the studies agrees with the 'true' input value to a precision of 0.05%. The fractional difference between the mean measured value and the 'true' value is 0.0005 ± 0.0006 and so we see no evidence of bias in the method. The shape of the measured lifetime distribution follows a Gaussian distribution.
In the case of the $\Lambda_b^0 \to p^+K^-$ lifetime the fractional difference between the mean measured and 'true' lifetime is 0.0018 ± 0.0009, also consistent with an unbiased measurement.

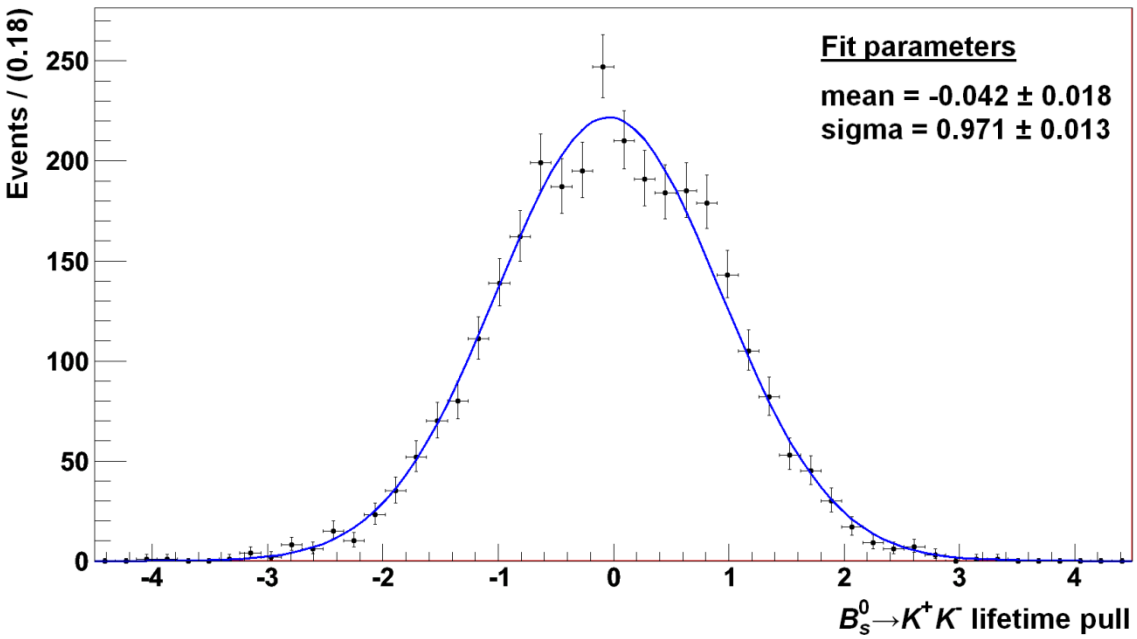

Figure 12 Pull distribution for the $B_s^0 \to K^+K^-$ lifetime for 3,000 toy studies fitted with a Gaussian distribution.

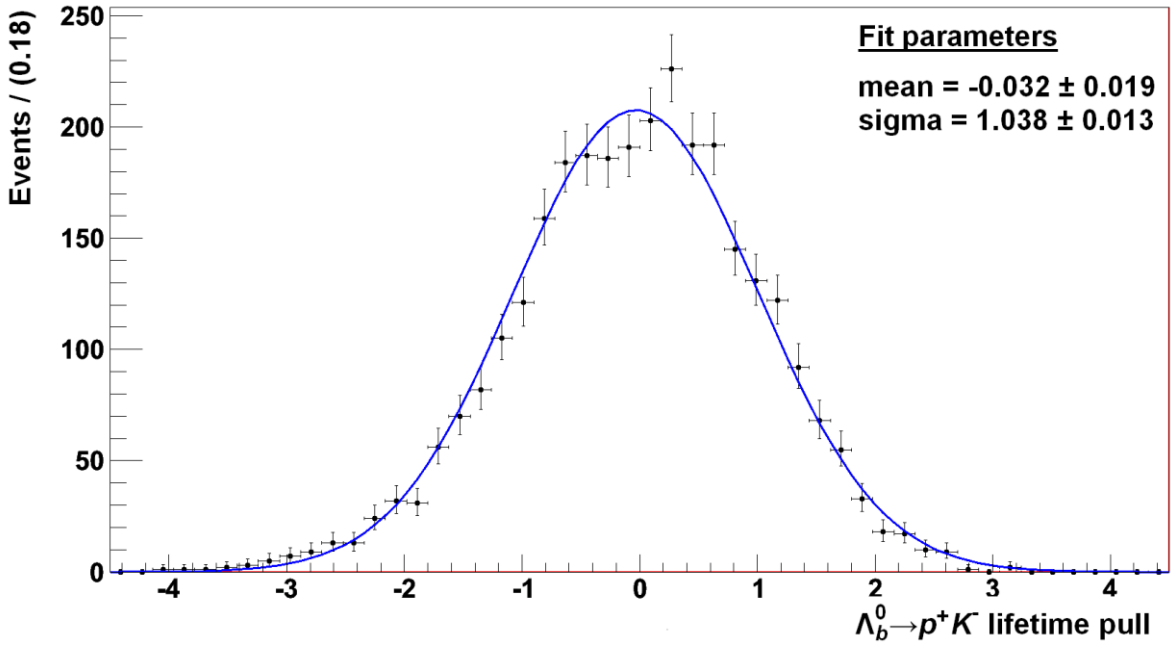

Figure 13 Pull distribution for the $\Lambda_b^0 \to p^+K^-$ lifetime for 3,000 toy studies fitted with a Gaussian distribution.

In Figure 12 and Figure 13 we see that the pulls for the $B_s^0 \to K^+K^-$ and $\Lambda_b^0 \to p^+K^-$ lifetimes follow Gaussian distributions and that the standard deviations of the pulls are both consistent with one. This is further evidence for the lifetime measurement being unbiased and also indicates that we are calculating our statistical errors correctly.

3.3 Statistics versus precision

Another study was performed to measure the effect of statistics on precision of the lifetime measurement. 200 toys were generated for each level of integrated luminosity. The precision was then taken as the width of the distribution of the measured lifetime. The results are presented in Table 8 along with a comparison with the precision offered by [16]. We see that after just a few days of data taking at nominal luminosity we should be able to measure the $B_s^0 \to K^+K^-$ lifetime to a precision of a few percent.

Number of $B_s^0 \to K^+K^-$ candidates	Integrated luminosity / pb^{-1}	Number of days of data taking at 2 fb^{-1} per year	Precision on $B_s^0 \to K^+K^-$ lifetime	Precision on $B_s^0 \to K^+K^-$ lifetime [16]
1000	33	6	11.6 %	-
5000	164	30	4.4 %	2.7 %
10,000	328	60	3.4 %	1.2 %
20,000	656	120	2.3 %	1.3 %
50,000	1,639	299	1.4 %	-
100,000	3,279	598	1.1 %	-

Table 8 Precision on the measurement of the $B_s^0 \to K^+K^-$ lifetime against number of true $B_s^0 \to K^+K^-$ candidates analysed for this analysis and the analysis presented in [16].

3.4 Proper lifetime binning

3.4.1 Bin shapes

As discussed in 2.4 the lifetime bins are chosen so that each bin contains approximately the same number of $B_s^0 \to K^+K^-$ candidates. We have performed toy Monte Carlo studies to examine the effect of changing the binning on the measured lifetime. For this study we use bins of equal width. The bin edges are given below in Table 9. The results of 1,000 studies each containing 328 pb^{-1} of data are presented in Table 10.

Bin	Lower edge / mm	Upper edge / mm	Share of total statistics
1	0.0	0.5	66 %
2	0.5	1.0	23 %
3	1.0	1.5	7 %
4	1.5	2.0	3 %
5	2.0	2.5	1.5 %
6	2.5	3.0	0.5 %

Table 9 Proper lifetime bins of constant width used in the toy Monte Carlo studies.

Decay mode	Input Lifetime / ps	Mean Measured Lifetime / ps	Precision
$B_s^0 \to K^+K^-$	1.4707	1.4775 ± 0.0018	3.1 %
$\Lambda_b^0 \to p^+K^-$	1.3840	1.411 ± 0.003	4.7 %

Table 10 The mean measured lifetimes from the toy Monte Carlo studies using proper lifetime bins of equal width.

We see that this choice of binning tends to bias the measured lifetimes to longer lifetimes while leaving the precision of the measurement relatively unaffected. We believe that the explanation for this bias is that at very low statistics the mass fit underestimates the number of $B_d^0 \to K^+\pi^-$ candidates by ascribing a larger share of the candidates to the channels $B_s^0 \to K^+K^-$ and $B_s^0 \to \pi^+K^-$. The long lifetime bins contain fewer candidates (as seen in Table 9) and so the number of $B_d^0 \to K^+\pi^-$ candidates is underestimated to a greater and greater extent as we move to longer proper lifetime. Since we measure the $B_s^0 \to K^+K^-$ and $\Lambda_b^0 \to p^+K^-$ lifetimes relative to the $B_d^0 \to K^+\pi^-$ lifetime this causes a bias to longer lifetime.

3.4.2 Number of bins

A second study has been performed to look at the effect of varying the number of proper lifetime bins on precision and mean fractional deviation. We have produced datasets containing 10,000 $B_s^0 \to K^+K^-$ candidates (328 pb^{-1}) and 1000 $B_s^0 \to K^+K^-$ candidates (33 pb^{-1}) for each choice of binning. Each individual study contains 200 such datasets (which is sufficient to estimate the spread of the data). The bins are chosen to contain an equal number of $B_s^0 \to K^+K^-$ candidates. The results of the study are presented in Table 11 and Table 12.

We see that, even at low statistics, increasing the number of proper lifetime bins improves precision. However, it should be noted that our cuts remove almost all background in our studies and this is will not be the case when studying real data. Further investigation into this effect is required which will be possible when we have larger LHC*b* simulation samples to work

on. We also note that altering the number of bins does not bias the lifetime measurement as is evident from Table 12.

Number of bins	Precision on B_s^0 lifetime for 33 pb^{-1}	Precision on B_s^0 lifetime for 328 pb^{-1}
3	13.6 %	4.0 %
4	12.5 %	3.6 %
6	12.1 %	3.4 %
8	11.2 %	3.3 %
12	10.8 %	3.3 %
24	10.6 %	3.2 %

Table 11 The effect of the number of proper lifetime bins on the precision of the measurement of the $B_s^0 \to K^+K^-$ lifetime at different statistics.

Number of bins	Mean fractional deviation from B_s^0 lifetime for 33 pb^{-1}	Mean fractional deviation from B_s^0 lifetime for 328 pb^{-1}
3	0.022 ± 0.010	-0.003 ± 0.003
4	0.014 ± 0.009	-0.002 ± 0.003
6	0.008 ± 0.009	0.0005 ± 0.0006
8	0.008 ± 0.008	0.000 ± 0.002
12	0.001 ± 0.008	-0.001 ± 0.002
24	0.004 ± 0.007	-0.002 ± 0.002

Table 12 The effect of the number of proper lifetime bins on the mean fractional deviation from the input $B_s^0 \to K^+K^-$ lifetime at different statistics.

4 LHC*b* Monte Carlo simulation studies

4.1 Results of the standard analysis

The analysis has been run on the LHC*b* Monte Carlo samples described in 1.2. The number of reconstructed events of each type used in the analysis are shown below in Table 13.

Channel	Number of successfully reconstructed candidates
$B_s^0 \to K^+K^-$	25,063
$B_s^0 \to K^-\pi^+$	25,722
$B_s^0 \to K^-\rho^+$	8,870
$B_d^0 \to K^+\pi^-$	25,711
$B_d^0 \to \pi^+\pi^-$	2,860
$\Lambda_b^0 \to K^-p^+$	12,169
$\Lambda_b^0 \to \pi^-p^+$	12,251

Table 13 The number of candidates for each channel reconstructed in the full physics simulation.

The events are re-weighted before the analysis in order to achieve the correct relative numbers of each channel according to the production cross sections and branching ratios. The full analysis described in Section 1 is then run on the data. The results are presented in Figure 14, Figure 15, Figure 16 and Table 14.

Looking at the plots and the measured lifetime we see that the analysis performs well when used on the full simulated data. The measured $B_s^0 \to K^+K^-$ and $\Lambda_b^0 \to p^+K^-$ lifetimes agree with the input values. We note also that the errors on the measured lifetimes agree well with the standard deviations from the toy studies with 10,000 $B_s^0 \to K^+K^-$ candidates. In the full LHC*b* simulation around 8,000 $B_s^0 \to K^+K^-$ candidates pass the cuts so we have comparable statistics in both cases. In Figure 14 we do not see any evidence of a $B_d^0 \to \pi^+\pi^-$ peak in the invariant mass spectra indicating that our cuts have almost completely removed this signal, as desired.

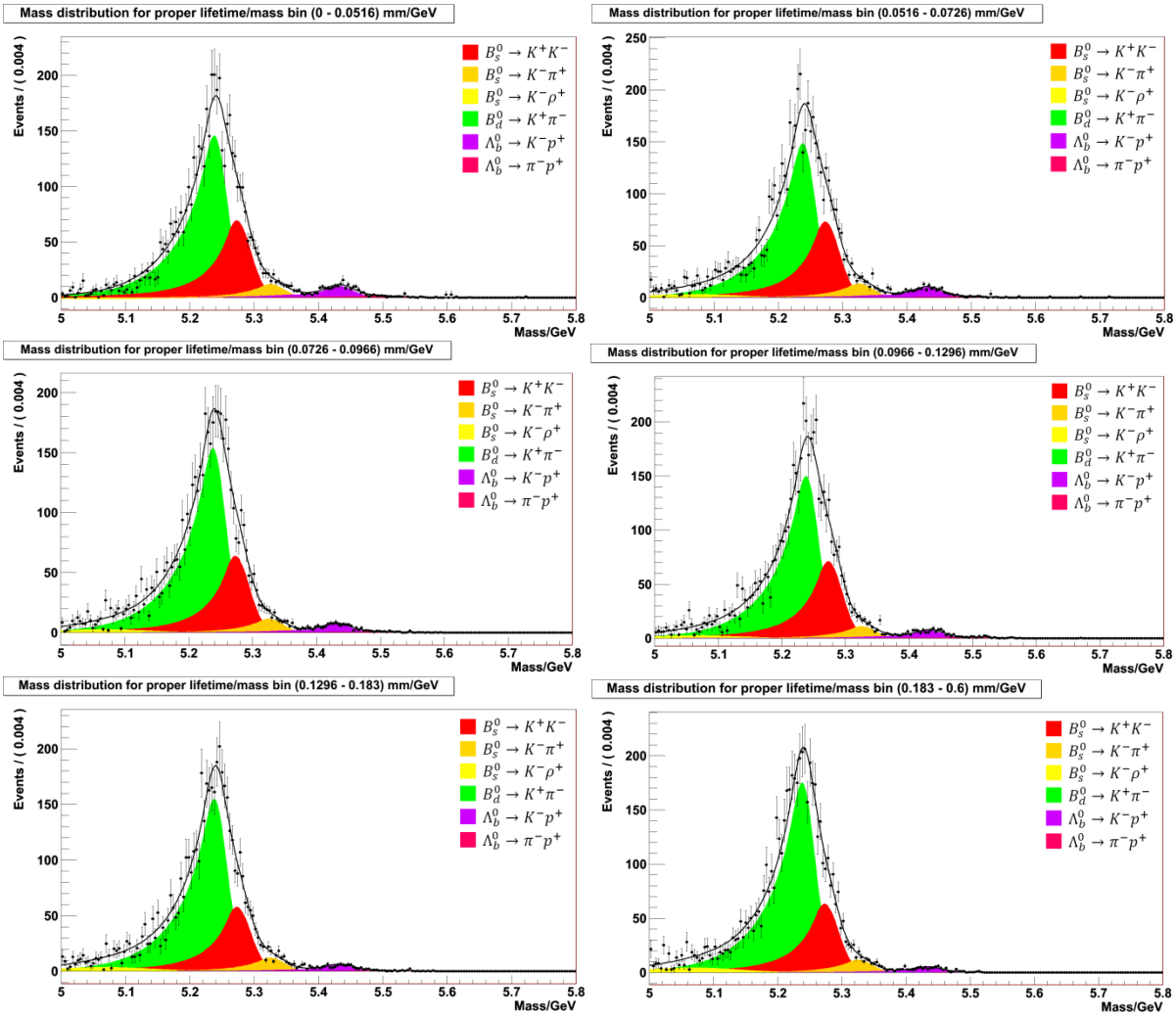

Figure 14 Invariant mass fits in bins of proper lifetime for simulated data.

Decay mode	Input Lifetime / ps	Measured Lifetime / ps
$B_s^0 \to K^+K^-$	1.461	1.40 ± 0.05
$\Lambda_b^0 \to p^+K^-$	1.229	1.19 ± 0.05

Table 14 The results of the analysis on simulated events.

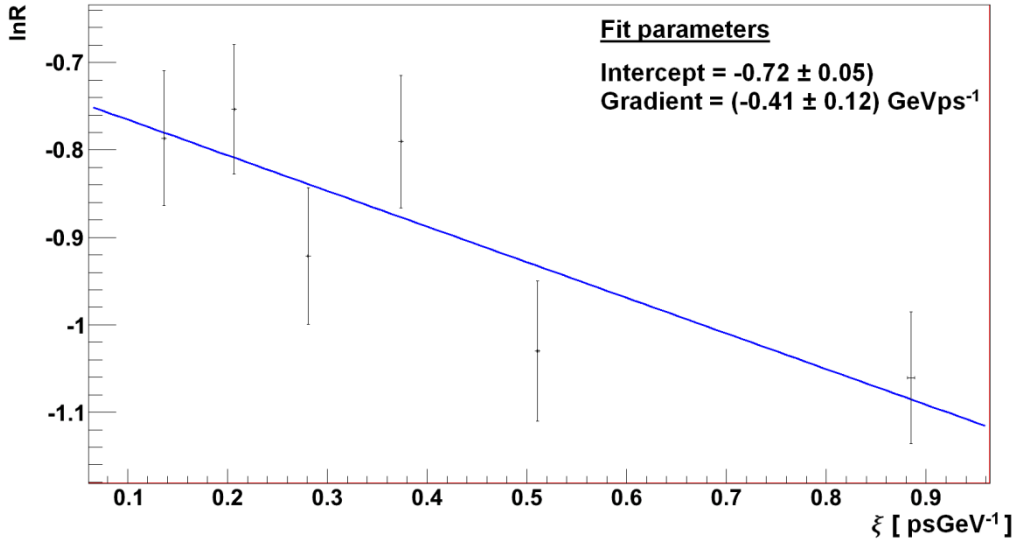

Figure 15 Plot of the natural log of the ratio of the yields of the decays $B_s^0 \to K^+K^-$ and $B_d^0 \to K^+\pi^-$.

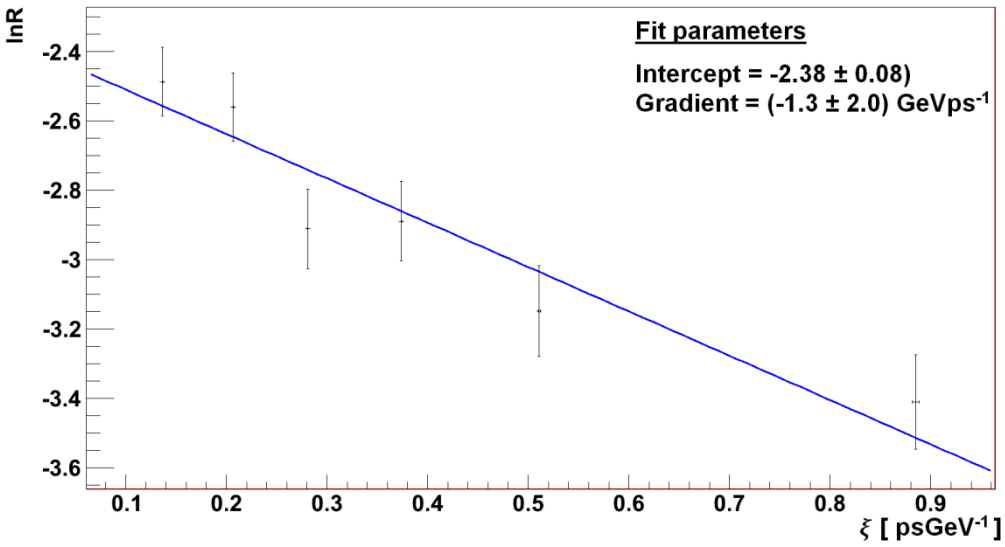

Figure 16 Plot of the natural log of the ratio of the yields of the decays $\Lambda_b^0 \to K^-p^+$ and $B_d^0 \to K^+\pi^-$.

4.2 Evaluation of systematic uncertainties

It is important to understand systematic effects that our method may impose on the results. We have already looked for those introduced by the invariant mass fit and the lifetime extraction with our toy study in Section 3. However, our simple toy model is not capable of measuring any biasing effect of the $H_b \to h^+h'^-$ selection. As discussed previously we hope to cancel many systematic effects, including those of the $H_b \to h^+h'^-$ selection, by making a relative, rather than absolute measurement of the $B_s^0 \to K^+K^-$ lifetime. However, this relies on the decays $B_s^0 \to K^+K^-$ and $B_d^0 \to K^+\pi^-$ having similar distributions of selection variables.

In Figure 7 we saw that the proper time dependence of selection acceptance is consistent with being equal for both channels. This result demonstrates that any bias introduced by differences between the selection variables will be small. However, it is necessary to estimate the scale of any such bias and this is presented below.

In the standard $H_b \to h^+h'^-$ offline selection (Table 1) we cut on transverse momentum, impact parameter significance, χ^2 of the vertex fit and distance of flight. We compare the distributions of these variables for our two channels in Figure 17, Figure 18, Figure 19, Figure 20, Figure 21 and Figure 22. These plots are calculated from the full LHC*b* Monte Carlo described in 1.2.

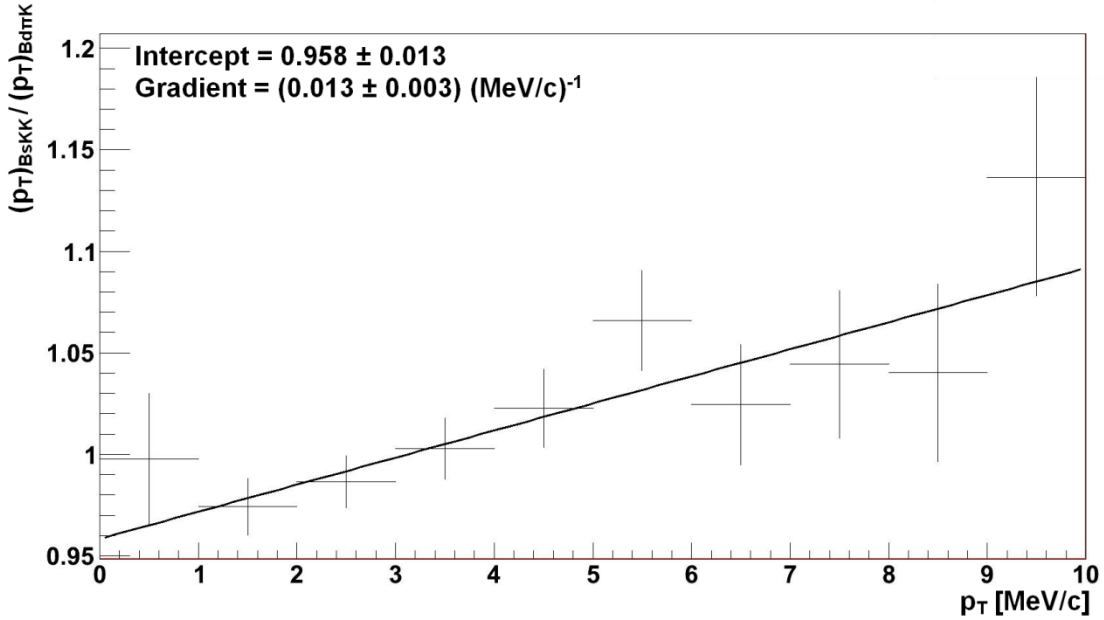

Figure 17 The ratio of the transverse momentum distributions of the daughter particles from the decays $B_s^0 \to K^+K^-$ and $B_d^0 \to K^+\pi^-$.

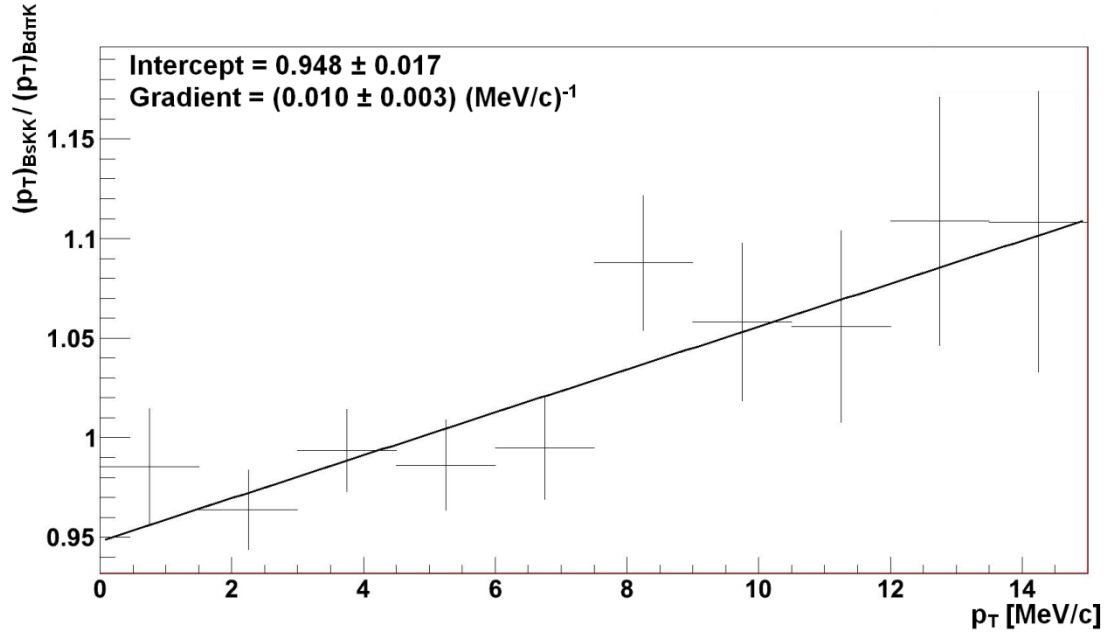

Figure 18 The ratio of the transverse momentum distributions of the B meson from the decays $B_s^0 \to K^+K^-$ and $B_d^0 \to K^+\pi^-$.

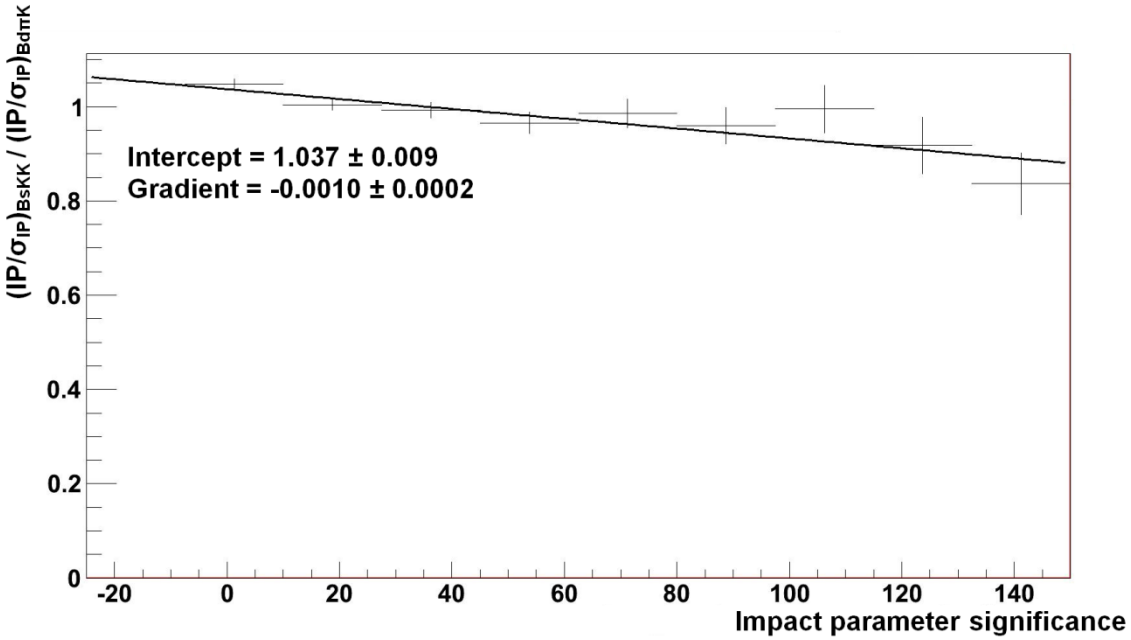

Figure 19 The ratio of the impact parameter significance distributions of the daughter particles from the decays $B_s^0 \to K^+K^-$ and $B_d^0 \to K^+\pi^-$.

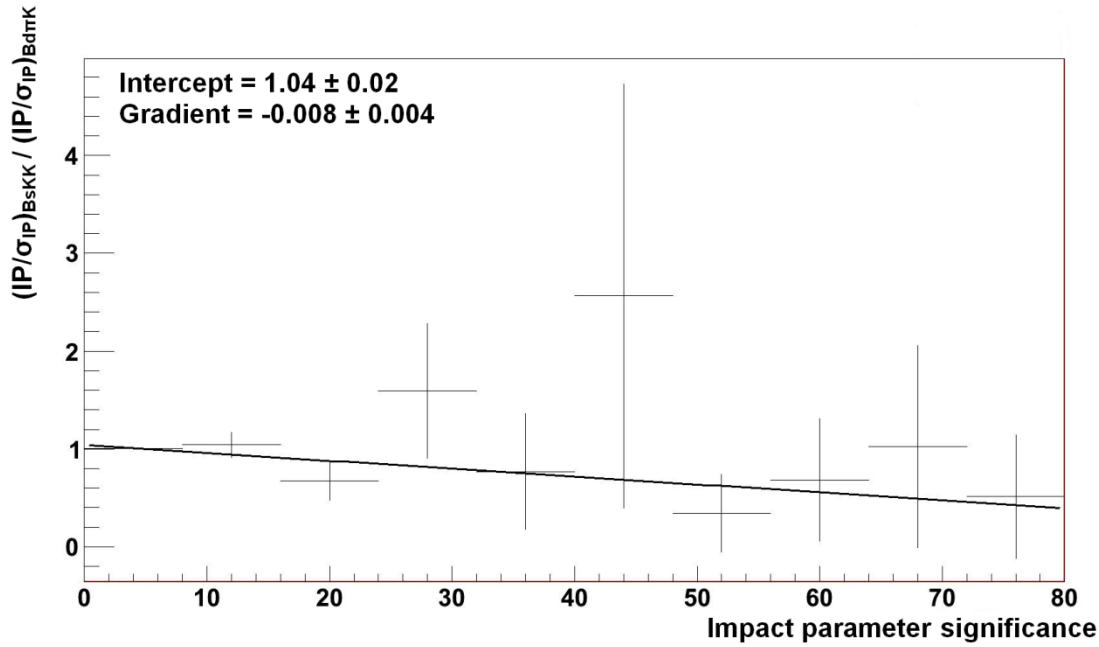

Figure 20 The ratio of the impact parameter significance distributions of the B mesons from the decays $B_s^0 \to K^+K^-$ and $B_d^0 \to K^+\pi^-$.

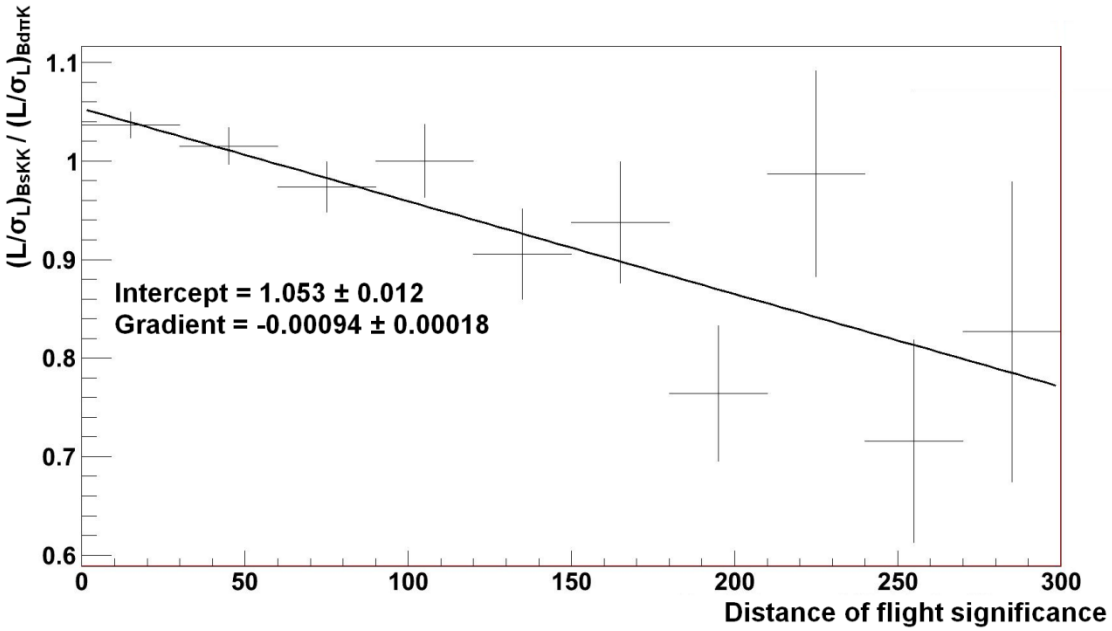

Figure 21 The ratio of the distance of flight significance distributions of the B meson from the decays $B_s^0 \to K^+K^-$ and $B_d^0 \to K^+\pi^-$.

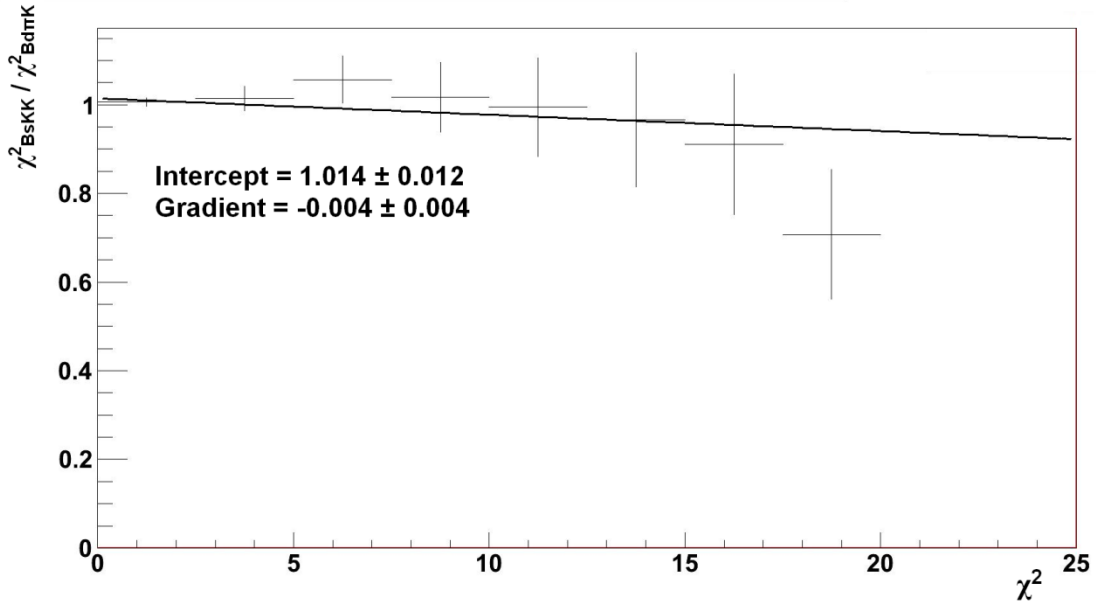

Figure 22 The ratio of the χ^2 distributions of the from the decays $B_s^0 \to K^+K^-$ and $B_d^0 \to K^+\pi^-$.

All these distributions are shown with the same number of candidates for each decay so we would expect flat lines at y = 1 if the distributions were the same for both channels. In the case of the transverse momentum distributions we see that $B_s^0 \to K^+K^-$ and $B_d^0 \to K^+\pi^-$ have very similar distributions since both show almost flat lines close to y = 1. However, there are significant differences between the impact parameter significance distributions and distance of flight significance distributions, and it is cuts on these variables which introduce the lifetime bias.

It is important to understand the effect of these differences on the final measured $B_s^0 \to K^+K^-$ lifetime. A study has been performed in order to give an estimate of the order of magnitude of

any effects. The study is performed as follows:

1) For each variable (transverse momentum, impact parameter significance, χ^2 and distance of flight) a straight line is fitted to the ratio of the distributions for $B_s^0 \to K^+K^-$ to $B_d^0 \to K^+\pi^-$.
2) We then perform the full lifetime analysis described above with the $B_s^0 \to K^+K^-$ events reweighted in order to force the ratio of the distributions of each variable to be equal to one.
3) The resulting lifetime is recorded.

For example, if the ratio of the $B_s^0 \to K^+K^-$and $B_d^0 \to K^+\pi^-$ B candidate transverse momentum distributions is fitted with straight line:

$$R(p_{T_B}) = Ap_{T_B} + B \tag{41}$$

Then each $B_s^0 \to K^+K^-$ candidate is given the weight:

$$w = \frac{1}{Ap_{T_B} + B} \tag{42}$$

The results are presented below in Table 15.

Variable with respect to which events are re-weighted	**Measured B_s^0 lifetime / ps**
$(IP/\sigma_{IP})^h$	1.46 ± 0.05
p_T^h	1.46 ± 0.05
p_{T_B}	1.50 ± 0.05
L_B/σ_{L_B}	1.46 ± 0.05
IP_B/σ_{IP_B}	1.52 ± 0.05
χ^2	1.47 ± 0.05

Table 15 Results of the re-weighting proceedure.

Looking at these results we see that the differences between the unmodified result ((1.46 ± 0.04) × 10^{-12} seconds) and these recalculated lifetimes are not significant within the available LHC*b* simulated event statistics. We see the largest deviation in the case of the impact parameter significance variable. This is as expected since in Figure 19 and Figure 20 we see that the impact parameter distributions for $B_s^0 \to K^+K^-$ and $B_d^0 \to K^+\pi^-$ differ significantly.

We can conclude that differences between the $H_b \to h^+h'^-$cut variables' distributions do not bias our lifetime measurement within current statistical uncertainty. We can also conclude that the differences between the impact parameter significance distributions may have the largest impact since selection criteria using these variables distort the proper lifetime distributions. We require larger simulated data studies in order to properly understand the scale of these biases. However, the agreement between the input value of the $B_s^0 \to K^+K^-$ lifetime and the measured value from simulated data presented in 4.1 suggests that any biases will be small.

5 Conclusions

In summary we have developed an analysis that allows us to make an unbiased measurement of the $B_s^0 \to K^+K^-$ lifetime. The lifetime is measured relative to the better constrained lifetime of the B_d^0 meson through comparison of decay channels $B_s^0 \to K^+K^-$ and $B_d^0 \to K^+\pi^-$. By taking a ratio of the proper lifetime distributions for these two decays we hope to eliminate many sources of systematic errors since both channels have the same topology and Feynman diagrams.

Toy simulation studies have demonstrated that the method does not introduce bias into the lifetime measurement. Further studies on LHC*b* Monte Carlo simulated events produce the result:

$$\tau_{B_s \to KK} = (1.40 \pm 0.05_{stat}) \text{ ps}$$

with

$$\tau_{B_s \to KK\ input} = 1.461 \text{ ps}$$

successfully reproducing the input value of the lifetime to within two standard deviations. This method is also capable of producing a measurement of the lifetime of the Λ_b^0 through the decay $\Lambda_b^0 \to K^-p^+$. However, in this case not all systematic errors will be eliminated since $\Lambda_b^0 \to K^-p^+$ and $B_d^0 \to K^+\pi^-$ have different topologies.

Due to the ability of this method to cancel un-quantified systematic effects it may be used early in data taking. Toy Monte Carlo studies have shown that this analysis is capable of measuring the $B_s^0 \to K^+K^-$ lifetime to a statistical precision of 10% within just a few days of data taking at design luminosity.

Planned further work on this analysis includes a study of effects of misalignment of the vertex locator at LHC*b*, an investigation into the selection acceptance for Λ_b^0 decays and a study to determine how this analysis will perform during early data taking. A more detailed toy model will be developed to include an impact parameter based selection and a background sample introduced into the full fit.

6 References

[1] The LHCb collaboration, The LHCb detector at the LHC, JINST 3 S08005 (2008).

[2] T.L.S. Group. The Large Hadron Collider – conceptual design. October 1995. CERN/AC/90-05(LHC).

[3] Y. Grossman, "The B_s width difference beyond the standard model", Phys. Lett. B 380 (1996) 99 [arXiv:hep-ph/9603244].

[4] A. Lenz and U. Nierste, "Theoretical update of $B_s - \overline{B_s}$ mixing", JHEP 0706 (2007) 072 [arXiv:hep-ph/0612167].

[5] M. Donega, "Measurement of the $B_s \to K^+K^-$ lifetime and extraction of $\Delta\Gamma_{CP}/\Gamma_{CP}$ at CDF Run II *and* Development of the ATLAS-SCT endcap modules", Ph.D. thesis (2006).

[6] K. Anikeev *et al.*, "*B* physics at the Tevatron: Run II and beyond", [arXiv:hep-ph/0201071].

[7] K. Hartkorn and H. G. Moser, "A new method of measuring Delta(Gamma)/Gamma in the B/s0 anti-B/s0 system", Eur. Phys. J. C 8 (1999) 381.

[8] The CDF Collaboration, Measurement of the $B_s^0 \to K^+K^-$ lifetime and extraction of $\Delta\Gamma_{CP}/\Gamma_{CP}$, CDF public note, 2006.

[9] http://www.slac.stanford.edu/xorg/hfag/osc/end 2005/

[10] T. Sjöstrand, S. Mrenna and P. Skands, "PYTHIA 6.4 Physics and Manual", JHEP 0605 (2006) 026 [arXiv:hep-ph/0603175].

[11] D. J. Lange, "The EvtGen particle decay simulation package", Nucl. Instrum. Meth. A 462 (2001) 152.

[12] E. Barberio, B. van Eijk and Z. Was, "PHOTOS: A Universal Monte Carlo for QED radiative corrections in decays", Comput. Phys. Commun. 66 (1991) 115.

[13] S. Agostinelli, *et al.*, "GEANT4 – a simulation tool kit," Nucl. Instrum. Meth. A, vol. 506, 2003, pp. 250303.

[14] V. V. Gligorov, J. Rademacker, Monte Carlo Independent Lifetime Fitting at LHCb in Lifetime Biased Channels, Technical Report CERN-LHCb-PUB-2007-053, 2007.

[15] M. Gersabeck, V. Gligorov, J. Imong, J. Rademacker, A Monte Carlo simulation free method of measuring lifetimes using event-by-event acceptance functions at LHCb, CERN-LHCb-PUB-2009-022, 2009.

[16] U. Kerzel, V. Gibson, Unbiased $B_s^0 \to K^+K^-$ lifetime measurement, CERN-LHCb-PUB-2009-024, 2009.

[17] C. Amsler *et al.,* (Particle Data Group), PL B667, 1 (2008) (URL: http://pdg.lbl.gov).

[18] A. Bates *et al.,* (CP Measurements Working Group, Gamma with Loops), Draft road map for charmless charged two-body B decays at LHCb, LHCb/2008-xx.

[19] A. Carbone *et al*., Charmless charged two-body B decays at LHCb, CERN-LHCb-PUB-2007-059.

[20] R. Forty, O. Schneider, RICH pattern recognition, LHCb/1998–40.

[21] J. E. Gaiser, Appendix-F Charmonium Spectroscopy from Radiative Decays of the J/ψ and ψ', Ph.D. Thesis.

[22] W. Verkerke, D Kirkby, The RooFit toolkit for data modelling, CHEP-2003-MOLT007, Jun 2003. 9pp.

[23] R. Brun, F. Rademakers, ROOT: An object oriented data analysis framework, Nucl. Instrum. Meth. A389:81-86, 1997.

[24] F. James and M. Roos, Minuit: A System for Function Minimization and Analysis of the Parameter Errors and Correlations. Comput. Phys. Commun., 10:343–367, 1975.